Received: 14 August 2023 | Revised: 3 January 2024 | Accepted: 2 February 2024

DOI: 10.1111/psyp.14544

PSYCHOPHYSIOLOGY SPR WILEY

ORIGINAL ARTICLE

Systemic neurophysiological signals of auditory predictive coding

Manuel Muñoz-Caracuel[1,2] | **Vanesa Muñoz**[1] | **Francisco J. Ruiz-Martínez**[1] | **Antonio J. Vázquez Morejón**[2,3] | **Carlos M. Gómez**[1]

[1]Department of Experimental Psychology, University of Seville, Seville, Spain

[2]Mental Health Unit, Hospital Universitario Virgen del Rocio, Seville, Spain

[3]Department of Personality, Evaluation and Psychological Treatments, University of Seville, Seville, Spain

Correspondence
Manuel Muñoz-Caracuel, Human Psychobiology Laboratory, Experimental Psychology Department, University of Seville, Calle Camilo José Cela, S/N, Sevilla 41018, Spain.
Email: mmunoz41@us.es;

Funding information
Spanish Agencia Estatal de Investigación (AEI), Grant/Award Number: PID2022-139151OB-I00; Agencia de Innovación y Desarrollo de Andalucía, Grant/Award Number: P20_00537

Abstract

Predictive coding framework posits that our brain continuously monitors changes in the environment and updates its predictive models, minimizing prediction errors to efficiently adapt to environmental demands. However, the underlying neurophysiological mechanisms of these predictive phenomena remain unclear. The present study aimed to explore the systemic neurophysiological correlates of predictive coding processes during passive and active auditory processing. Electroencephalography (EEG), functional near-infrared spectroscopy (fNIRS), and autonomic nervous system (ANS) measures were analyzed using an auditory pattern-based novelty oddball paradigm. A sample of 32 healthy subjects was recruited. The results showed shared slow evoked potentials between passive and active conditions that could be interpreted as automatic predictive processes of anticipation and updating, independent of conscious attentional effort. A dissociated topography of the cortical hemodynamic activity and distinctive evoked potentials upon auditory pattern violation were also found between both conditions, whereas only conscious perception leading to imperative responses was accompanied by phasic ANS responses. These results suggest a systemic-level hierarchical reallocation of predictive coding neural resources as a function of contextual demands in the face of sensory stimulation. Principal component analysis permitted to associate the variability of some of the recorded signals.

KEYWORDS

ANS, auditory processes, ERPs, fNIRS, predictive coding, systemic response

1 | INTRODUCTION

Predictive coding is a growing theoretical framework in cognitive neuroscience that traces its origins to the idea of unconscious inference proposed by von Helmholtz (1867) for visual perceptual processing. It postulates that our brain is not merely a passive information processing organ, but an active self-organized neural system that continuously generates and updates internal models of the world (generative models) to effectively minimize prediction errors, enabling adaptive behavior in response to environmental demands while minimizing surprise and

energy consumption (Friston, 2010). Since the seminal work of Rao and Ballard (1999) on predictive coding in the visual cortex, this theory has gained extensive theoretical and empirical support in two primary application domains, perception, and decision-making (Ficco et al., 2021). According to this view, perception can be seen as an active and Bayesian inferential process that depends on the comparison of probabilistic predictions (prior) with incoming sensory information (likelihood), resulting in the so-called *prediction error*, a measure of the magnitude of this difference that is used to appropriately adjust and update the final percept (posterior) through the interconnection of different levels of the cortical hierarchy (Hohwy, 2012; Knill & Pouget, 2004).

Mismatch negativity (MMN) is an event-related potential (ERP) generated in response to rare or infrequent variations in regular sensory stimulation that occurs even in the absence of voluntary attention or conscious effort (Näätänen et al., 1978; Näätänen et al., 2007). Empirical evidence has linked MMN to the predictive coding framework as a bottom-up prediction error, signaling the discrepancy between incoming auditory input (likelihood) and auditory memory representations (prior) embodied in top-down predictions. This mechanism allows for the adjustment and updating of the final percept (posterior) within a hierarchical cortical model (Garrido et al., 2009).

Different competing hypotheses have been proposed for the generation of MMN, such as the *memory-trace hypothesis*, which proposes that the MMN arises from the active comparison of the current input with a memory trace of recently encountered sounds (Näätänen & Winkler, 1999), or the *neural adaptation hypothesis*, which proposes that the generation of the MMN depends on basic physiological phenomena such as habituation, refractoriness, or neural fatigue in response to repeated input, which would explain the increased responsiveness of neurons to infrequent stimuli (Jääskeläinen et al., 2004; May et al., 1999). However, the *predictive coding account* has emerged as a harmonious and integrative model that addresses the limitations of these previous hypotheses. It has proven to be a satisfactory and unifying theory for explaining the generation of MMN across the vast heterogeneity of experimental paradigms used to elicit it (Fitzgerald & Todd, 2020; Garrido et al., 2009; Winkler, 2008).

Sources of the MMN signal have been consistently identified in temporal and frontal cortical regions using a variety of source localization methods (Molholm et al., 2005; Opitz et al., 2002). Specifically, the primary auditory cortex, superior temporal gyrus (STG), and inferior frontal gyrus (IFG) have been identified as hierarchically interrelated cortical regions in a bottom-up propagation pathway, as indicated by dynamic causal modeling (DCM) studies (Garrido et al., 2008). In addition, a second propagation pathway from the auditory cortex to motor cortical areas has been proposed by single-trial EEG-fMRI analysis (Li et al., 2019). In general, right hemisphere activation has been shown to predominate over the left hemisphere (Levänen et al., 1996; Recasens & Uhlhaas, 2017; Wang et al., 2021).

Classical oddball paradigms based on pitch or duration deviants have been most commonly used in MMN research (Tervaniemi, 2022), but more complex oddball paradigms, such as those based on auditory patterns, have also been employed in MMN research for their ability to evidence how the neural representation of auditory stimuli encodes not only the physical features of repetitive stimuli but also the abstract attributes derived from common invariant features of the individual events (Korzyukov et al., 2003; Saarinen et al., 1992; Tervaniemi et al., 1994). In recent years, these paradigms have continued to be of important interest and have been studied extensively in the MMN literature, providing further support for the predictive coding view of MMN (Hsu et al., 2015; Li et al., 2019; Ruiz-Martínez et al., 2021; Wacongne et al., 2011). Furthermore, auditory patterns have shown to be potentially suitable for eliciting other ERPs related to top-down processes, such as the contingent negative variation (CNV) and the consecutive post-imperative negative variation (PINV) (Ruiz-Martínez et al., 2022), which are slow ERPs that have been scarcely addressed within the framework of predictive coding so far. CNV and PINV represent two phases (deflection and recovery) of the same slow and long-lasting negative wave, and they are more commonly observed in active forewarning reaction time tasks following a warning stimulus (cue) and a deviant imperative stimulus (target), respectively (Kathmann et al., 1990; Walter et al., 1964). The CNV has been related to cognitive processes such as expectancy or motor readiness, whereas the PINV has been linked to cognitive processes such as uncertainty or reappraisal of ambiguous contingencies, with its amplitude being higher for deviant stimuli (Arjona et al., 2014; Klein et al., 1996; Ruiz-Martínez et al., 2022). Both ERPs are typically studied under conscious attentional demands in active experimental tasks. However, their elicitation during passive or involuntary encoding of sensory information has been little analyzed and discussed in the literature until very recently (Ruiz-Martínez et al., 2022).

Despite the extensive research on the MMN, its many facets and underlying mechanisms have not yet been fully uncovered (Grent-'t-Jong & Uhlhaas, 2020), and its interpretation continues to be debated (Sussman et al., 2014). Similarly, there are still unknowns about the cognitive determinants and psychological significance of the less-studied slow evoked potentials CNV and PINV, their possible role during passive or involuntary sensory

information encoding, and their relationship with other neurophysiological responses. Furthermore, the interplay between the MMN and other sequentially related ERPs, such as the P300 and the reorienting negativity (RON), is not equally addressed in the MMN literature (Escera & Corral, 2007; Horváth et al., 2008), partly due to the great heterogeneity of paradigms used for the MMN elicitation and interpretation.

On the other hand, although embodied cognition is a relevant conceptual issue within the predictive coding framework (Allen & Friston, 2018; Seth & Friston, 2016), little empirical research has addressed this question in an integrative manner. Recent work from our group (Muñoz et al., 2022; Muñoz-Caracuel et al., 2021) has shown the complex relationship between the peripheral and central nervous system (CNS) during sensory information encoding and, to our knowledge, only a few studies have investigated these systemic responses using oddball paradigms. Lyytinen et al. (1992) found that neither heart rate (HR) nor skin conductance response (SCR) seemed to correlate with the MMN elicitation, whereas elicitation of the P300 component would be associated with a higher SCR. Other studies with oddball paradigms had focused their analysis on HR, mostly related to the P300 component. These studies characterized the cardiac response as an early deceleration, proposed as an orienting response, and a late acceleration, reflecting cognitive load, with larger amplitudes for deviant or target stimuli (Simons et al., 1998). Guerra et al. (2016) found a dependence between the P300 and the HR response, associating HR decelerations with larger P300 responses. However, information about autonomic responses to higher complexity oddball paradigms is lacking, and questions within the predictive coding framework remain unapproached.

Lastly, various studies have investigated the neural underpinnings of passive and active deviance and target detection using ERPs and functional magnetic resonance imaging (fMRI) with the classic auditory oddball paradigm (Justen & Herbert, 2018; Kim, 2014); however, to the best of our knowledge, there are neither previous studies using higher complexity oddball paradigms to analyze passive–active discrimination nor multimodal neurophysiological approaches that include autonomic nervous system (ANS) measures together with ERPs and brain hemodynamic activity recordings, which could expand our comprehension about predictive coding phenomena.

For these reasons, the present study aims to explore the systemic neurophysiological correlates of predictive coding processes, dissociating between passive and active auditory processing. To this aim, a novelty auditory oddball paradigm specifically designed to fit within the predictive coding framework is used. This paradigm is based on previous work from our laboratory (Ruiz-Martínez et al., 2021), with some modifications to ensure predictive updating on a trial-by-trial basis, distinguishing between passive and active responses. A multimodal neurophysiological approach, using electroencephalography (EEG) and functional near-infrared spectroscopy (fNIRS), is employed. Simultaneous EEG-fNIRS recordings have the advantage of combining the time course and spatial location brain activity analyses in a noisy-free and comfortable environment, taking advantage of the complementary temporal and spatial resolution properties of each technique to examine the cortical activity in a more comprehensive way. Additionally, a set of peripheral physiological measures, usually used as autonomic markers, are used to explore the ANS response to auditory stimulation, such as electrodermal activity (EDA), HR, heart rate variability (HRV), respiration rate (RSP), and a spectral analysis of the peripheral pulse signal (PPG). This comprehensive approach attempts to enhance our understanding and characterization of systemic neurophysiological responses to prediction errors within the predictive coding framework. Principal components analysis (PCA) would permit to assess in an exploratory manner the possible interrelationships of the recorded physiological variables.

2 | MATERIALS AND METHODS

2.1 | Participants

A sample of 32 healthy subjects (12 males and 20 females, 29 right-handed and 3 left-handed) aged between 19 and 36 years old (mean = 28.31 ± 3.87 SD) were recorded in both experimental conditions. For the EEG data, five subjects were excluded from the analysis for the passive condition, and three for the active condition, due to technical issues during the EEG recording or low signal-to-noise ratio with a high percentage of trials removed by excess voltage (described in the Data Analysis section). For fNIRS and autonomic response data, no subjects were excluded.

The study was approved by the Bioethical Committee of the Junta de Andalucía. Subjects did not report any neurological disease or auditory impairment and they were recruited from a middle socioeconomic background. The experiments were conducted with the informed and written consent of each participant, following the Helsinki Protocol.

2.2 | Stimuli

An auditory complex MMN paradigm based on previous work from our group (Ruiz-Martínez et al., 2021) was

used, with some modifications. The experiment was programmed using PsychoPy v.2021.1.2 free software package (Peirce, 2009). The auditory stimuli were edited using Audacity free software package, v.3.0.0.

The stimuli consisted of trials of four consecutive pure auditory tones (from T1 to T4) presented in an ascending or descending frequency pattern (50–50%, randomly counterbalanced within subjects) that was occasionally broken in the last tone (T4) of the trial (Figure 1a). Each tone lasted 200 ms (20 ms rise–fall time). The interstimulus interval (ISI) was 100 ms, and the intertrial interval (ITI) was 1900 ms. In total, there were four different types of trials from the combination of congruent–incongruent T4 and ascendent–descendent sequence (Figure 1b). In order to have enough time for the manifestation of the responses and baseline recovery in the slow neurophysiological signals used in this study (fNIRS and ANS signals), there was an additional constraint that a deviant trial (D) should be followed by at least three consecutive standard trials (S) (12 s equivalent) (Figure 1d).

In this experimental setting, in addition to the level of uncertainty about T4 type (congruent–incongruent), there is an extra level of uncertainty about sequence type (ascendent–descendent) that forces the brain to update its auditory predictions trial by trial. The fact that the same auditory tone (T4) appears as congruent or incongruent depending on the prior auditory tones (T1–T3) limits an MMN generation explanation based on neuronal adaptation or habituation processes and highlights the local predictive coding processes required in each trial.

Two conditions were used in this study. First, a passive condition in which the participants were asked to watch a muted film and ignore the tones. Second, after a brief break, an active condition in which the participants were asked to pay attention to the tones and to respond within the ITI time window (1900 ms post-T4) in each of the trials by pressing the up or down arrow on the keyboard, depending on whether the fourth tone (T4) of the sequence had a lower or higher frequency than the previous one (T3), trying to combine precision and speed in their responses. The task was divided into four blocks of 60 trials, separated by a short break, to prevent the effects of fatigue.

In the active condition, the first three tones (T1–T3) acted as a warning or cue stimuli, whereas T4 tone was the imperative or target stimulus. There was a training period with an explanatory video, followed by a test trial with visual feedback. The experimental task did not start until the participant achieved 10 consecutive correct answers in the test trial. The order of conditions, first passive and then active condition, was intentionally kept constant across participants to avoid possible interference or conditioning factors from the active to the passive condition in the auditory processing system.

Auditory stimuli were presented through two speakers (Dell, model A215), positioned on either side of the participant's head at a comfortable listening volume of 60 dB (measured with a Velleman-DVM1326 level sound meter). Participants were seated in front of a screen during the experiment. In total, each condition was composed of 240 trials, with an 80–20% ratio (192 standards, 48 deviants) between standards and deviants, respectively.

2.3 | Signal acquisition

2.3.1 | Electroencephalography

The EEG was recorded using active electrodes (ActiCAP) from 13 scalp sites mainly distributed along the midline (AFz, Fz, FCz, Cz, CPz, Pz, C1, C2, Fp2, Fz9, Fz10, Tp9, and Tp10) (Figure 1c) with a Brain Vision V-Amp DC amplifier (Brain Products, Munich, Germany). The electrode impedance was kept below 20 kΩ. The left mastoid was used as the reference. DC amplification gain was 20,000, and the sampling rate was 1000 Hz. Data acquisition was done using BrainVision Recorder 1.20 (Brain Products).

2.3.2 | Functional near-infrared spectroscopy

The fNIRS signal was recorded using a NIRScoutXP device (NIRx Medical Technologies, Glen Head, NY, USA) with 16 LED sources and 22 detectors (14 common detectors +16 short separation channel detectors) placed along the frontotemporal areas of both sides of the scalp, obtaining a total of 58 channels (Figure 1c). The fNIRS uses two different wavelengths (760 and 850 nm) and avalanche photodiodes, which provide a high sensitivity to the optical signal. The source–detector distance was 3 and 0.8 cm for short separation channels. The sampling rate was 3.91 Hz. Data acquisition was accomplished with NIRStar v.14.2 software.

2.3.3 | Peripheral signals

For the recording of the autonomic peripheral signals, an MP160 (BIOPAC Systems, Goleta, CA, USA) with four amplifier modules (PPG-100C, EDA-100C, ECG-100C, and RSP-100C) was used to obtain the PPG, EDA, ECG, and RSP signals, respectively.

The pulse was recorded through a photoplethysmograph (TSD200 transducer with a wavelength of 860 ± 60 nm infrared light) placed on the index finger of the left hand. EDA was obtained using bipolar Ag-AgCl finger electrodes placed on the ring and middle fingers of

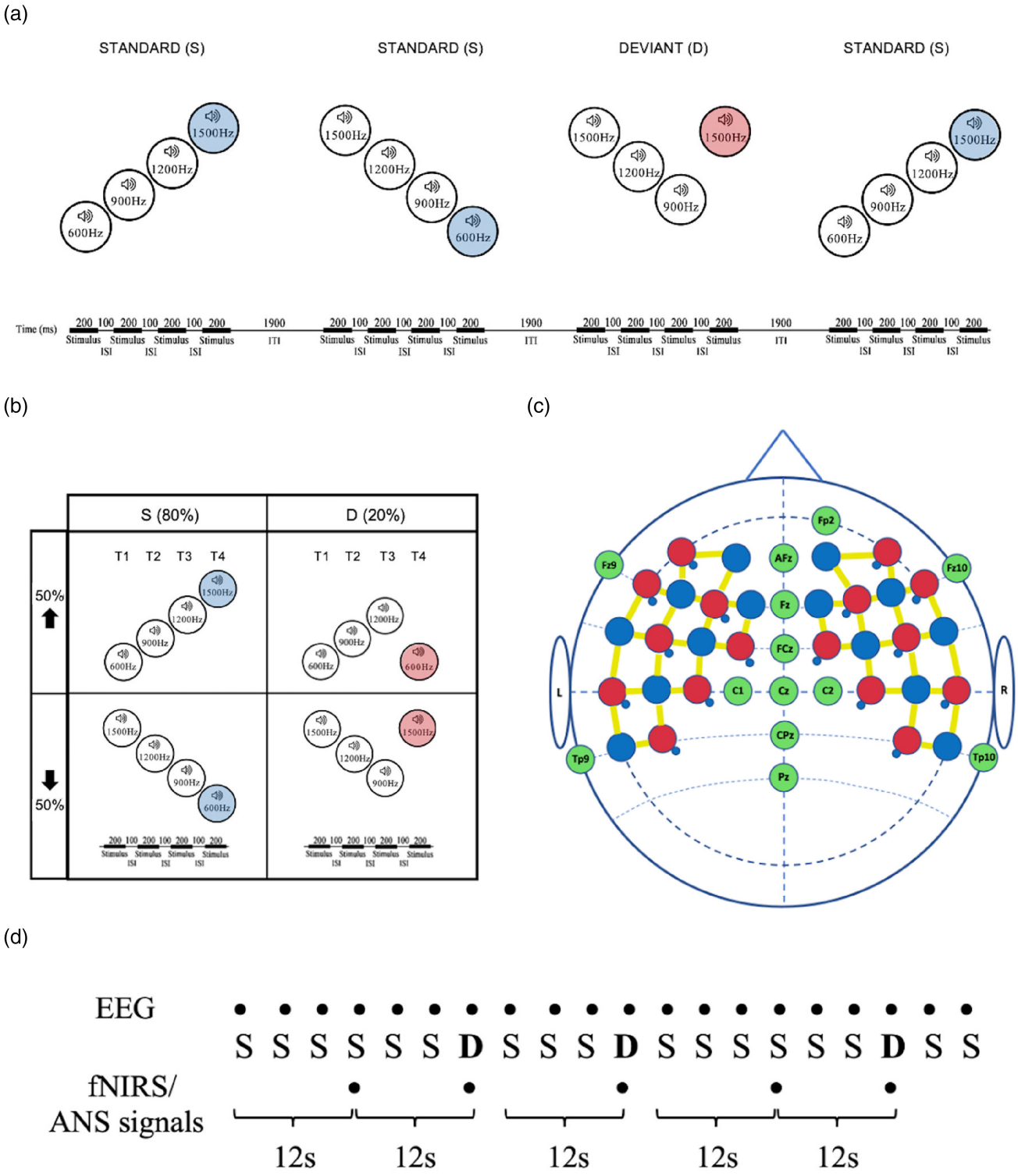

FIGURE 1 (a) Experimental design exemplification. Standard (S) and deviant (D) trials are composed of four consecutive tones that differ only in the congruence or incongruence of the fourth tone (T4) with respect to the sequence of the three previous tones. (b) The box shows the four different trials used in the stimulation protocol, as product of the interaction between type of trial (standard–deviant, 80–20% randomized) and type of sequence (ascendent–descendent, 50–50% randomly counterbalanced within subjects). T1–T4 represent the four consecutive auditory tones of each trial. The colors blue and red in T4 represent congruent and incongruent auditory tones, respectively. (c) Distribution of near-infrared spectroscopy (fNIRS) optodes and EEG recording electrodes. Red circles indicate fNIRS sources, blue circles fNIRS detectors, and green circles EEG channels. Yellow linear segments between sources and detectors indicate fNIRS channels. Overlapping small blue circles indicate the location of fNIRS short separation channels. (d) Exemplification of standard (S) and deviant (D) trial sequences given the experimental constraints. The dots above and below each trial represent the eligible trials for statistical analysis in EEG and fNIRS/ANS signals, respectively. Note that for fNIRS/ANS signals, conversely to EEG signals, eligible standard trials require at least three consecutive preceding standard trials (12 s equivalent).

the left hand. ECG was acquired using three Ag-AgCl lead electrodes (positive, negative, and ground, TSD203 transducer) placed on the left wrist, right wrist, and right ankle, respectively. RSP was recorded through a transducer band placed on the chest (TSD201 transducer), which allows measurement of changes in thoracic circumference that occur with breaths.

The amplification gain was set as 100 in PPG, 5 in EDA, 1000 in ECG, and 10 in the RSP amplifiers. The sampling frequency was 1000 Hz. Data acquisition was performed using AcqKnowledge v.5.0.1 software (BIOPAC Systems). Data filtering and processing were performed in AcqKnowledge v.5.0.1 (BIOPAC Systems), MATLAB R2019b (MathWorks), Ledalab (Benedek & Kaernbach, 2010), HEPLAB (Perakakis, 2019), and KARDIA (Perakakis et al., 2010) software packages.

2.4 | Data analysis

2.4.1 | Electroencephalography

EEG recordings were analyzed with EEGLAB v.14.1.1 and MATLAB 2017b software. A high-pass (0.1 Hz cut-off) and a low-pass (30 Hz cut-off) filter were applied to the EEG recording. To correct the EEG for eye blinking, ocular movements, and muscle artifacts, an independent component analysis (ICA) was computed from the non-epoched data. These components were removed, and the EEG signal was posteriorly reconstructed (mean = 3.5 ± 0.93 SD, range 2–7).

The signal amplitudes in the electrodes Fp2, F9, and F10 were used to detect eyeblink artifacts and ocular movements and they were removed from the posterior analysis.

Epochs were segmented in time windows from −100 to 2900 ms. All the epochs in which the EEG amplitude exceeded ±80 microvolts were rejected for analysis. In the passive condition, the mean of accepted standard and deviant trials were as follows: 179.63 ± 14.01 SD (range: 125–192) and 45.41 ± 2.61 SD (range: 39–48), respectively, whereas in the active condition, 179.62 ± 18.2 SD (range: 77–128) trials were accepted for the standard and 45.41 ± 4.54 SD (range: 33–51) for the deviant trials. ERPLAB software was used to average the resulting epochs depending on the type of trial (standard or deviant) for each subject, both in the passive and active paradigms. The STUDY function of EEGLAB was used to compare the standard and deviant trials for all the participants in each experimental condition. This comparison was performed using the EEGLAB fieldtrip toolbox (Oostenveld et al., 2011) to perform a cluster mass permutation analysis, with an alpha level of $p \leq .05$ and computing 2000 randomizations.

Two different time windows were selected for the analysis. First, −50 to 400 ms post-T4, with the aim of analyzing prototypical latencies of the MMN and P300 components, and second, the full epoch (from −100 to 2900 ms post-T1), to study the ERPs elicited for each type of trial without any theoretical apriorism.

The differences observed between the ERPs elicited by the passive and active conditions in the latency between T1 and T4 motivated an additional comparison between both paradigms averaging both types of trials (standard and deviant) in this time window to assess possible differences in CNV amplitude between active and passive conditions.

2.4.2 | Functional near-infrared spectroscopy

To ensure baseline recovery and lack of interference in the response signal to standard trials by adjacent deviant trials, only those standard trials that had at least three prior and two posterior standard trials were extracted through a custom MATLAB script for statistical data analysis (Figure 1d). Thus, the final mean of standard trials for analysis was as follows: 21.06 ± 3.34 SD (range: 19–36) in the passive condition and 22.84 ± 3.28 SD (range: 19–34) in the active condition. Then, the fNIRS raw data were imported into the HOMER2 v.2.8 toolbox (Huppert et al., 2009) and MATLAB 2017b software for preprocessing. First, for pruning the noisy channels, the function *enPruneChannels* was performed. This algorithm removes channels with extreme values that saturate the signal (levels 0.03–2.0), or those channels that present a high standard deviation (an SNR value of 5 was fixed to obtain a coefficient of variation of 17). For the reduction in the signal motion artifacts, the function *hmrMotionCorrectionWavelet* was applied, with an interquartile range of 1.5. This function has proven to be quite robust in decreasing motion artifacts through wavelet decomposition (Brigadoi et al., 2014; Cooper et al., 2012; Molavi & Dumont, 2010). For the remaining artifacts, the function *hmrMotionArtifact* (SDThresh = 15; AMPThresh = 0.7; tmotion = 0.5; and tmask = 1.0) was used. The signal was bandpass filtered between 0.01 and 0.5 Hz with the function *hmrBandpassFilt*. Additionally, the *enPCAFilter* function was applied, selecting one principal component to remove from the data. The function *hmrSSR* was also applied, which regresses the activity in the short separation channels from the activity of the standard channels, in order to eliminate the contribution of the extracerebral signal from the cortical recorded signal. The function *enStimRejection* was also employed to remove remaining artifacts in the signal from −2 to 10 s around the stimulus.

The hemoglobin concentrations were obtained employing the modified Beer–Lambert law with a differential partial pathlength factor of 6.0 for 760 nm and 5.0 for the 850 nm wavelength (Scholkmann et al., 2010).

The filtered and preprocessed signal was imported into SPM-fNIRS v.3 toolbox (Ye et al., 2009) for statistical analysis and topographical visualization after applying a MATLAB custom code for data compatibility. Channel positions were rendered onto the ICBM-152 cortical template surface introducing the spatial MNI coordinates of the montage. The data were downsampled to 1 Hz and whitened using the AR model (Purdon & Weisskoff, 1998). The GLM for each subject was then fitted to the channel-specific oxyhemoglobin (HbO) responses. The first-level design matrix included four regressors (standard and deviant events for passive and active conditions) convolved with a basis set consisting of the canonical HRF and its temporal and dispersion derivatives, which allowed us to consider the variability in the delay of the peak of the response. One sample *t*-test contrast was made for standard and deviant events in the passive and active conditions, whereas paired samples *t*-test contrasts were made for the comparison between events and conditions. Individual topographic images for each of the contrasts were made by interpolating the channel-wise contrast on a 3D triangular mesh (2562 vertices) of a canonical scalp surface. Finally, second-level fNIRS group analysis was implemented as a random-effects analysis via SPM12 (Tak et al., 2016), using one-sample *t*-test from all the individual 3D contrast images. The resulting *t*-test at the group level was represented as a *T*-statistic map; firstly, unthresholded to allow a visual inspection of the topographical cortical activation tendencies, and thresholded at p FWE-corr $<.05$ to highlight significantly activated regions over a canonical scalp surface for the passive and active conditions separately.

2.4.3 | Peripheral signals

As in the fNIRS analysis, to ensure baseline recovery of the slow autonomic measures, only those standard trials that had at least three preceding and two posterior standard trials were extracted using a custom MATLAB script for statistical data analysis (Figure 1d).

The PPG signal was analyzed by power spectral density (PSD) analysis. Using a custom script in MATLAB, the raw signal was extracted in a time window of 10 seconds post-T4, considering the variables condition (active–passive) and type of trial (standard–deviant). The PSD was then calculated for each extracted signal using the *plomb* function. The frequency range for the analysis was chosen according to previous research, from 0.04 to 0.15 Hz for LF, and from 0.15 to 0.4 Hz for HF (Ishbulatov et al., 2020; Kiselev & Karavaev, 2020; Muñoz et al., 2022). These values were normalized by the division of the total power and multiplied by 100. An additional analysis was performed in a larger time window (720 s), considering only the conditions (passive–active), following the same procedure described above. For the statistical analysis, an ANOVA was performed with trial (standard–deviant) and condition (passive–active) as factors for the 10 s analysis and with conditions only for the 720 s analysis. The variables analyzed for this signal were the LFnu, HFnu, and the LF/HF ratio.

The EDA signal was analyzed with the Ledalab software (Benedek & Kaernbach, 2010) using the continuous decomposition analysis (CDA; Benedek & Kaernbach, 2010) function, which allows decomposing the EDA signal in its phasic and tonic components. The phasic and tonic measurements were then extracted following the SCR analysis guidelines (Boucsein et al., 2012) in a time window from 1 to 5 s and a minimum SCR amplitude of 0.01 μS. Statistical analysis was performed using an ANOVA with type of trial and condition as factors, considering the early response in the EDA signal. The variables extracted from Ledalab for the statistical analysis were the SCR (i.e., the time integral of the driver function in the window selected divided by window length) and, lastly, the tonic activity, related to the SCL (skin conductance level).

For cardiac analysis, first, the ECG signal was extracted and processed with HEPLAB software (Perakakis, 2019) using the *PanTompkins* function (Pan & Tompkins, 1985) to find the R peaks for each subject. The signal was visually inspected to avoid misdetections and to detect ectopic beats. Second, the R peak values were converted to interbeat intervals (IBIs) and exported to the KARDIA software (Perakakis et al., 2010). The cardiac parameters analyzed in KARDIA were phasic cardiac responses (PCR) and HRV. For the PCR, a mean of the conditions, type of trial, and subjects was performed to select the first negative and positive peak post-T4 stimulus (Figure S1); thus, a time window of 0.5 s was selected around the peaks. The ANOVA was performed for each peak considering both conditions (passive–active) and type of trial (standard–deviant) as factors. An additional analysis that only included the conditions (passive–active) choosing a larger time window of 720 s was also performed. For HRV, due to the minimum time required for a reliable estimation of this measure, only the conditions (passive–active) were analyzed in a 720 s time window. The HRV was calculated for the time and frequency domain, following the software parameters, in which the IBIs series is interpolated by cubic spline at 2 Hz, detrended by a constant with a Hanning

windowing function, and calculated through the fast Fourier transform (FFT) at a 16 AR order. And finally, the frequency spectrum is divided into three bands: VLF (0–0.04 Hz), LF (0.04–0.15 Hz), and HF (0.15–0.5 Hz). The variables analyzed in the ANOVA for the frequency domain were the VLF, LF, HF, LFnu, HFnu, and the LF/HF ratio; and for the time domain, RMSSD (root mean square of successive differences) and the SDNN (standard deviation of normal to normal). The condition was included as a factor in the ANOVA.

The RSP signal was analyzed through the respiration rate. First, the signal was band-pass filtered (0.05–1 Hz) in the acqKnowledge software to improve peak detection. Then, in MATLAB, using a custom script, the signal was selected for a time window of 720 s post-conditions (passive–active), considering the slow changes in the signal. The rate was then calculated using the *diff* function and converted to beats per minute (bpm). Finally, to obtain more reliable results, the artifact values of the signal were rejected with the function *isoutlier*. For the ANOVA, the condition was included as a factor.

2.4.4 | Principal component analysis (PCA)

In order to study the possible interrelationships of the recorded physiological variables, a PCA was computed (Gorsuch, 1983). PCA is obtained from correlation matrices of recorded variables, therefore a pattern of covariation would be obtained, and no causality would be determined. PCA was computed by mixing the four conditions (standard active and passive plus deviant active and passive; $N = 112$ cases). Only variables that showed statistical significance in the comparisons of standard versus deviant, and that were present in active and passive conditions, were introduced in the analysis. The nine variables that fulfilled these preconditions were as follows: ERP_CNV_FCz, ERP_PINV_FCz, fNIRS_HbO_R_STG, fNIRS_HbO_L_STG, fNIRS_HbO_R_MFG, fNIRS_HbO_L_MFG, fNIRS_HbO_FP, ANS_HR_PCR, and ANS_EDA_SCR. The electrode considered for the ERP variables was FCz, and the time window selected ranged from 100 to 900 ms post-T1 for the CNV, and 1250 to 2000 ms post-T1 for the PINV. For fNIRS variables, preprocessed signal from HOMER2 was averaged across subjects for each identified ROI, and HbO signal amplitude ranged from 3 to 8 seconds was averaged. For ANS variables, latencies selected for PCA analysis are the same as previously mentioned in the Data Analysis section.

The Varimax rotation was applied to facilitate the physiological interpretation of a reduced number of components. Components with eigenvalues >1 were selected for further processing. Hair et al. (1998) proposed for loading components of a variable to be ≥0.51 in order to consider that a given empirical variable is significantly related to the computed component, for a number of 112 cases. This criterion imposes a very strict threshold, higher than the significance level applied to correlation coefficient, due to the fact that factor loadings present larger standard errors than correlations (Hair et al., 1998). A more flexible approach involves calculating the Euclidean distance between each empirical variable based on the loading components derived from the PCA. When the Euclidean distances between two variables are small, it means that those variables are located close to each other in the PCA space, thus sharing common variability. This alternative analysis complements the thresholding method proposed by Hair et al. (1998), providing a different perspective on how a specific component accounts for the variance within a particular set of signals.

3 | RESULTS

3.1 | Behavioral measures

Task performance was 189/192 (98%) ± 5.54 SD mean hit rate for standards and 47/48 (99%) ± 1.84 SD for deviants. The mean reaction time for standards was 667 ± 104 ms SD and 764 ± 133 ms SD for deviants. Differences in reaction time between type of trials reached significant results [$t(31) = 7.27$; $p < .001$; Dev > Std]. No significant differences were found between type of trials for hit rate [$t(31) = 0.21$; $p = .836$].

3.2 | Electroencephalography

For the sake of simplification, due to the well-known frontocentral distribution of the ERPs of interest (Kathmann et al., 1990; Näätänen et al., 2007; Walter et al., 1964) and the maximum peak amplitudes found for all the analyzed ERPs on this channel, only results from FCz channel are reported (for further details on the response of other channels, see Supplementary Materials, Figures S2–S6).

Figure 2 shows the ERPs elicited in the short time window (post-T4) in the FCz electrode for the passive and active conditions, respectively, after averaging each standard and deviant trial. The gray shaded areas correspond to the latencies at which the difference between standards and deviants was statistically significant ($p \leq .05$) according to the cluster-mass permutation analysis. An MMN was obtained in the passive condition, elicited between 100 and 200 ms post-T4 in response to deviant trials, whereas a P300 component was observed in the active condition, elicited around 220–320 ms post-T4 in response to the deviant trials. MMN and P300

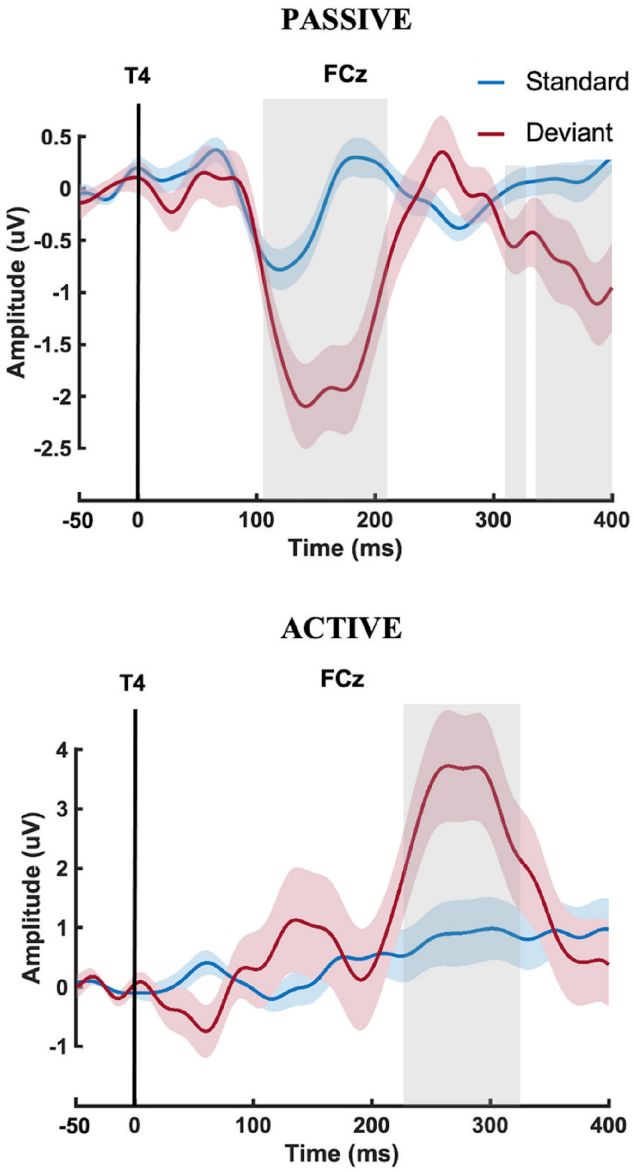

FIGURE 2 Comparison computed for the short time window (post-T4) between the standard and deviant trials in the FCz electrode for the passive and active conditions. The latencies at which the cluster-mass permutation analysis found significant differences ($p \leq .05$) are indicated by shaded gray areas. The blue and red shaded areas represent the standard error (SE) for standard and deviant trials, respectively.

response in other electrodes are displayed in Figures S3 and S5.

The entire epoch is shown in Figure 3. In addition to the MMN and P300 components shown in the previous figure for the passive and active conditions, a CNV component is observed in both conditions, between T1 and T4 onset, which will be the subject of further analysis. Interestingly, this figure also shows a PINV component elicited around 1200–2500 ms post-T1 in both conditions, reaching statistically significant differences between both types of trials around 1200–1600 ms post-T1 in the passive condition, and between 1270 and 1730 ms post-T1 in the active condition, with a higher ERP amplitude response for the deviant trials. The PINV presented similar dynamics and topography in both conditions (Figure 3 and Figures S2 and S4).

Figure 4 shows the ERP cluster mass comparison of the passive and active conditions for the average of the standard and deviant trials in the latency between the T1 and T4. This comparison showed a statistically significant difference in the CNV response between conditions, in the latency of 420–900 ms post-T1, with a more pronounced negativity in the active condition.

3.3 | Functional near-infrared spectroscopy

Effects of standard and deviant trials were identified at the group level using random-effects analysis (Tak et al., 2016). Four contrast images per subject, containing the effects of standard and deviant events for passive and active conditions, were computed from the HbO response by applying spatial interpolation to the channel-wise contrast value.

T-statistic maps, unthresholded and thresholded at $p < .05$ (family-wise error corrected for multiple comparisons over all scalp voxels/vertices), of standard and deviant contrast images were computed from the HbO responses and plotted on a canonical scalp surface for both the passive and active conditions in Figures 5 and 6, respectively. In the passive condition (Figure 5), no suprathreshold regions are identified for standard events, whereas a significant increase in HbO concentration in the right superior temporal area is observed for deviant events (peak-level $T = 3.58$; p FWE-corr = .036; cluster-level p FWE-corr = .046), and a trend is also found in the left superior temporal area for deviants, but it does not survive the multiple comparison correction (peak-level $T = 3.20$; p uncorr = .002; p FWE-corr = .081). In the active condition (Figure 6), greater and distinctive topographic HbO concentration changes for standard and deviant events are observed compared with the passive condition, with a significant increase in HbO concentration in the right medial frontopolar area for standard events (peak-level $T = 3.72$; p FWE-corr <.001; cluster-level p FWE-corr = .031) and both the left middle frontal area (peak-level $T = 5.53$; p FWE-corr <.001; cluster-level p FWE-corr <.001) and, to a lesser extent, the right middle frontal area (peak-level $T = 4.29$; p FWE-corr = .008; cluster-level p FWE-corr = .008) for deviant events.

No significantly activated cortical regions were obtained from the contrast image containing the effect of the comparison between types of trials (deviant > standard) for any condition (see Figure S7). An additional contrast image containing the effect of the comparison between conditions

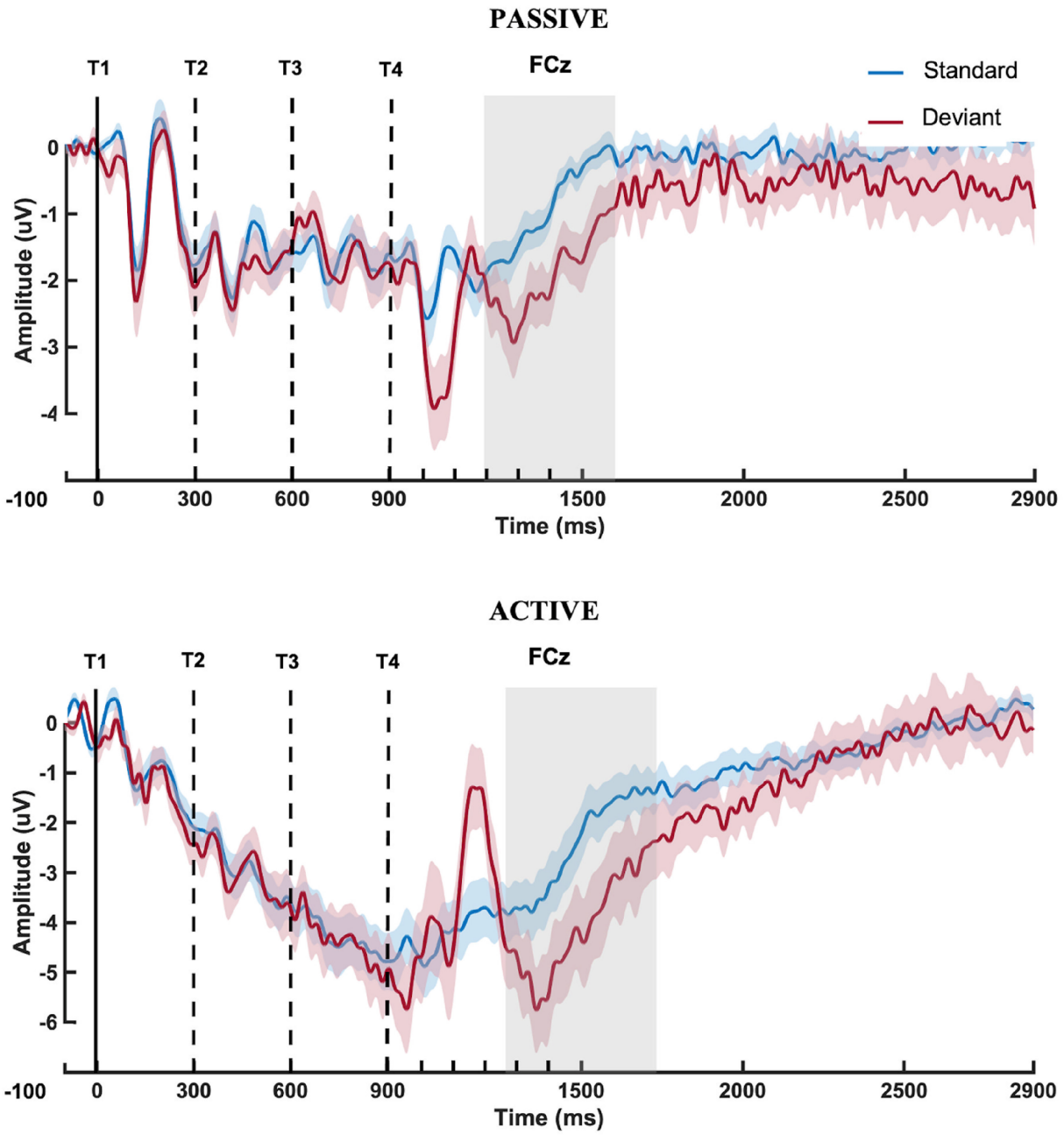

FIGURE 3 Comparison computed for the long time window between the standard and deviant trials in the FCz electrode for the passive and active conditions. The latencies at which the cluster-mass permutation analysis found significant differences ($p \leq .05$) are indicated by shaded gray areas. Note the similar dynamics of the PINV in the passive and active conditions. The blue and red shaded areas represent the standard error (SE) for standard and deviant trials, respectively.

(active > passive) was computed from the HbO response for standard and deviant events, respectively (Figure 7). For standard events, a non-statistically significant HbO superiority over the frontopolar area is observed for the active condition. For deviant events, a significant superiority of HbO concentration over the left middle frontal area is observed for the active condition compared to the passive condition (peak-level $T = 3.53$; p FWE-corr = .001; cluster-level p FWE-corr = .043), whereas a non-statistically significant superiority of HbO concentration over the temporal region of both cortical hemispheres is observed for the passive condition. For standard and deviant events taken together, a significantly activated cortical region in the left MFG was found from the Active > Passive contrast (see Figure S8).

3.4 | Peripheral signals

The EDA phasic activity for the passive and active conditions in the driver signal from the CDA decomposition is

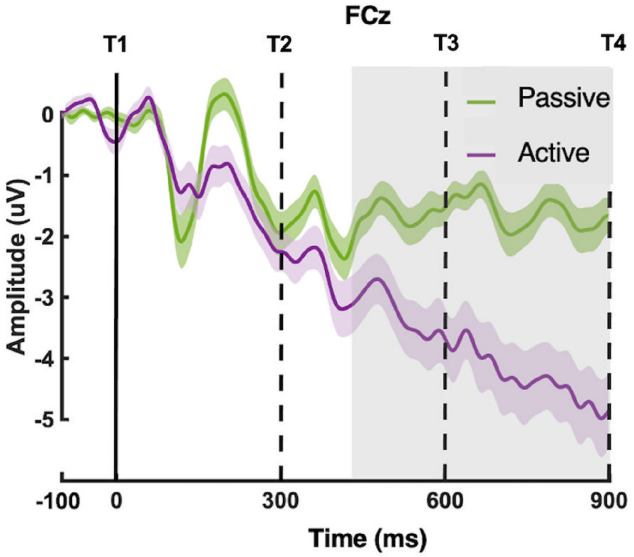

FIGURE 4 Comparison computed between the passive and active conditions for the time window from T1 to T4. The ERPs show the voltage obtained by averaging the standard and deviant trials in each condition, in the latency previous to T4, for the FCz electrode. The latencies at which the cluster-mass permutation analysis found significant differences ($p \leq .05$) are indicated by shaded gray areas. The green and purple shaded areas represent the standard error (SE) for the passive and active conditions, respectively.

shown in Figure 8a,b, respectively, where a notable amplitude increase is observed for deviant trials in the active condition. The ANOVA for the SCR showed an effect of the condition [F (1, 31) = 14.33; $p = .001$; $\eta^2 = 0.316$; observed power = 0.956; Passive < Active], type of trial [F (1, 31) = 13.12; $p = .001$; $\eta^2 = 0.297$; observed power = 0.939; Std < Dev], and interaction [F (1, 31) = 6.09; $p = .019$; $\eta^2 = 0.164$; observed power = 0.666]. This effect is given by the difference between standard and deviant trials in the active condition ($p = .001$; Std < Dev). EDA tonic activity (SCL) is shown in Figure 9a. SCL results revealed greater activity in the active condition [F (1, 31) = 122.31; $p < .001$; $\eta^2 = 0.603$; observed power = 1.00; Passive < Active] and also an interaction between condition and type of trial [F (1, 31) = 4778; $p = .036$; $\eta^2 = 0.134$; observed power = 0.563], which is given by the difference between the standard and deviant trials in the active condition ($p = .018$; Std < Dev).

The cardiac response for the passive and active conditions is shown in Figure 8c,d, respectively, where a marked early decreased response is observed for deviant trials in the active condition. The ANOVA for the negative peak showed an effect of condition [F (1, 31) = 12.74; $p = .001$; $\eta^2 = 0.291$; observed power = 0.933; Passive > Active], stimulus [F (1, 31) = 11.29; $p < .001$; $\eta^2 = 0.349$; observed power = 0.977; Std > Dev], and Condition x Stimulus [F (1, 31) = 4.38; $p < .002$; $\eta^2 = 0.269$; observed power = 0.905]. This effect is given by the difference between the standard and deviant trials in the active condition ($p < .001$; Std > Dev). For the positive peak, the ANOVA shows no effect of condition or stimulus. For the 720 s HR analysis, the ANOVA showed a significant effect of the condition [F (1, 31) = 32.02; $p < .001$; $\eta^2 = 0.508$; observed power = 1.00; Passive < Active], with a higher HR in the active condition (Figure 9b). For the HRV, the ANOVA only showed an effect for the HF [F (1, 31) = 8.999; $p = .005$; $\eta^2 = 0.225$; observed power = 0.828; Passive > Active] (Figure 9c).

For the RSP rate in the analyzed 720 s time window, the ANOVA showed a significant effect of the condition [F (1, 31) = 22.80; $p < .001$; $\eta^2 = 0.424$; observed power = 0.996; Passive < Active], with a higher respiration rate in the active condition (Figure 9d).

The PSD of the PPG signal analysis showed an effect of condition for the LFnu [F (1, 31) = 7.191; $p = .012$; $\eta^2 = 0.188$; observed power = 0.738; Passive < Active] and HFnu [F (1, 31) = 5.735; $p = .023$; $\eta^2 = 0.156$; observed power = 0.641], but not effect for the stimulus in the 10 s post-T4 analysis. Similarly, in the 720 s time window analysis by condition, the ANOVA only showed an effect of condition in the LFnu (Figure 9e) [F (1, 31) = 6.459; $p = .016$; $\eta^2 = 0.172$; observed power = 0.692]. For further details about the autonomic responses, see Supplementary Materials, Figure S9, which shows the continuous performance of the HR and the HF/LF response of the HRV for the 720 s time windows, and the PSD of the PPG for the 10 s and the 720 s time windows.

3.5 | Principal component analysis

Table 1 shows the loading components of the four extracted components. The variance of HbO in frontal and frontopolar regions was explained by the C1 variance. Slow CNV and PINV ERPs were related to HR as indicated by C2. The C3 explained the variance associated with HbO in left and right STG. The variance explained by C4 was associated only with the SCR variability.

The results from the Euclidean distance analysis are shown in Figure 10, where the interrelationship between variables based on the PCA analysis is visually highlighted. This graphical representation complements the PCA results mentioned above.

4 | DISCUSSION

The results showed some similar and dissimilar neurophysiological responses to pattern stimulation violation in the passive and active conditions, but still congruent with the predictive coding view of perception as an active inferential brain process. ERPs and fNIRS responses showed significantly greater

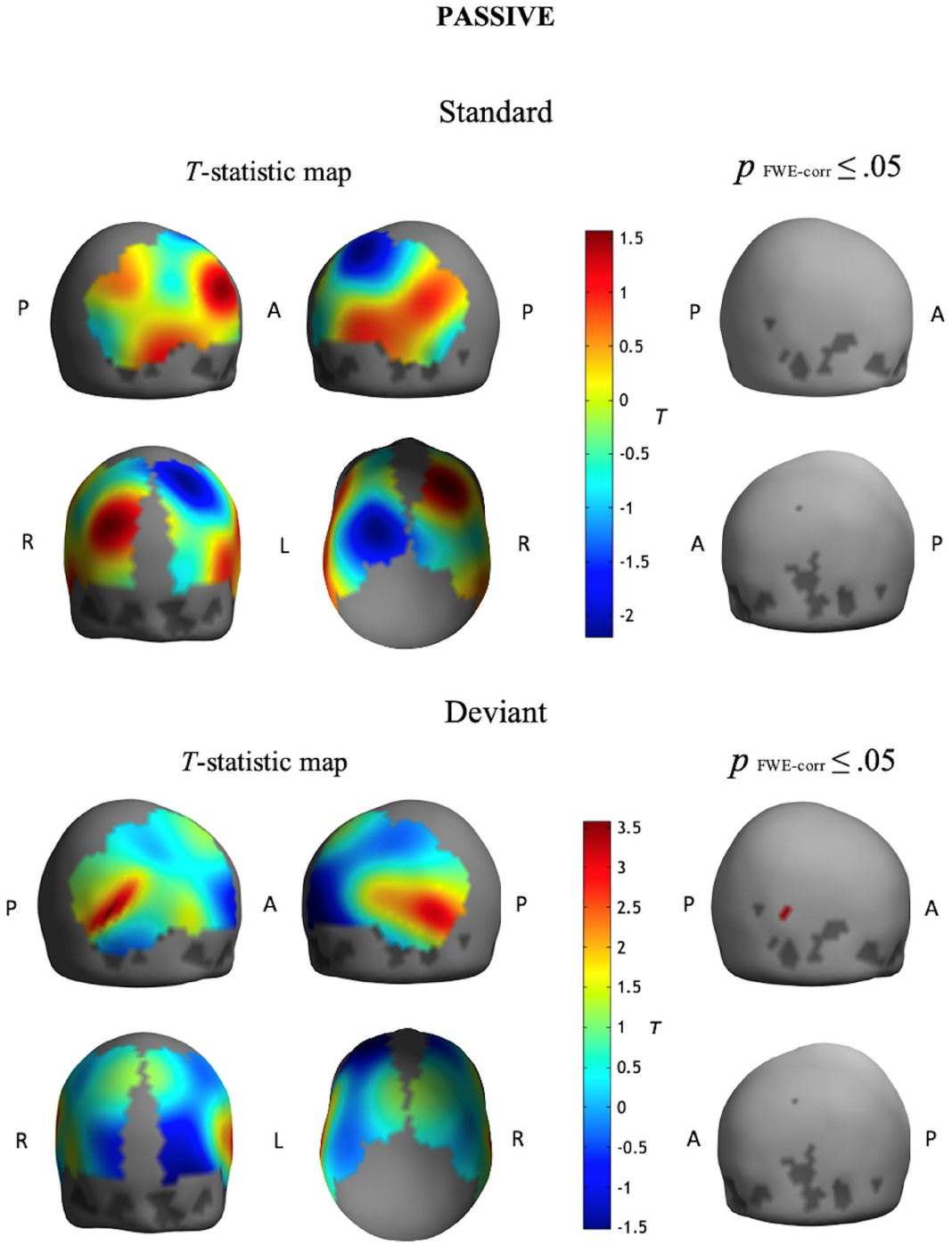

FIGURE 5 *T*-statistic maps unthresholded (left) and thresholded at *p* FWE-corr <.05 (right), derived from standard and deviant contrast images, respectively, and computed from the HbO responses for the passive condition. Note the HbO concentration increase to deviant trials in regions corresponding to superior temporal gyrus (STG) for the passive condition. A: anterior; P: posterior; L: left; R: right.

amplitudes for deviants compared to standards in both conditions, although the ERP components and fNIRS topographic response differed significantly for the active and passive conditions. In the autonomic responses, none of the measures show sensitivity to pattern stimulation violation in the passive condition, whereas the SCR signal from the EDA and the HR displayed significant reactivity for deviants in the active condition. Overall, higher-amplitude responses and biomarkers of sympathetic activity were found for the active condition in the neurophysiological recorded measures.

4.1 | Behavioral measures

In the active condition, the average hit rate was close to 99%, evidencing good comprehension and commitment

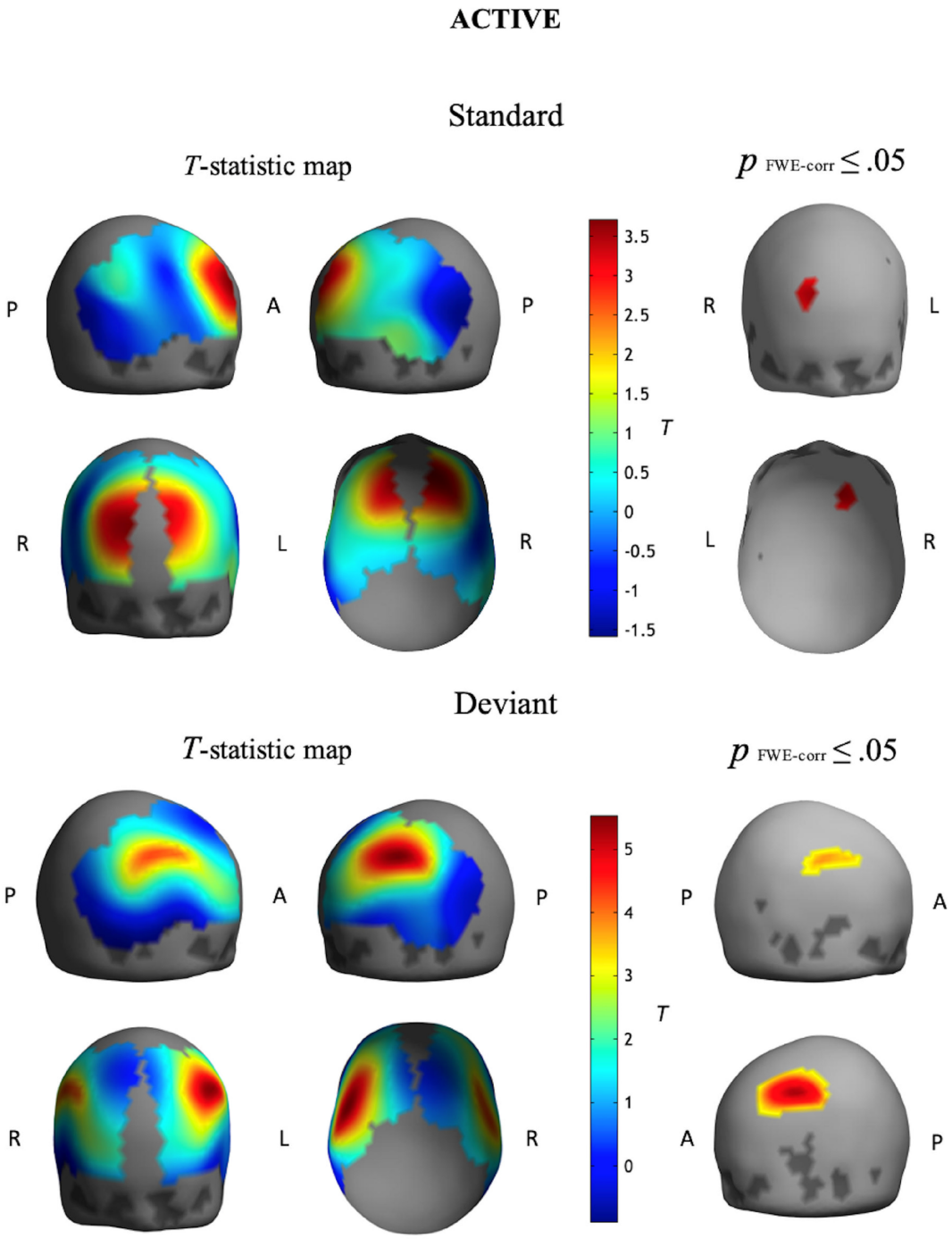

FIGURE 6 T-statistic maps unthresholded (left) and thresholded at *p* FWE-corr <.05 (right), derived from standard and deviant contrast images, respectively, and computed from the HbO responses for the active condition. Note the HbO concentration increase to deviant trials in regions corresponding to middle frontal gyrus (MFG) for the active condition. A: anterior; P: posterior; L: left; R: right.

from the participants to the task demands. Longer reaction times were found for the responses to deviants, similar to the RTs increase to invalidly cued targets in the Posner paradigm (Arjona et al., 2014; Posner, 1980; Vossel et al., 2006), suggesting the presence of higher-order cognitive processes anticipating the motor responses to standards, and/or inhibition of the anticipated motor response to T4 induced by the prior T1-T3 sequence in deviant trials.

4.2 | Electroencephalography

In the short latency ERP analysis, an MMN was found in response to deviant trials in the passive condition, whereas a P300 was found in the active condition. These distinct evoked potentials as a function of the task demands on each condition could be interpreted as the two sides of the same coin in a predictive processing

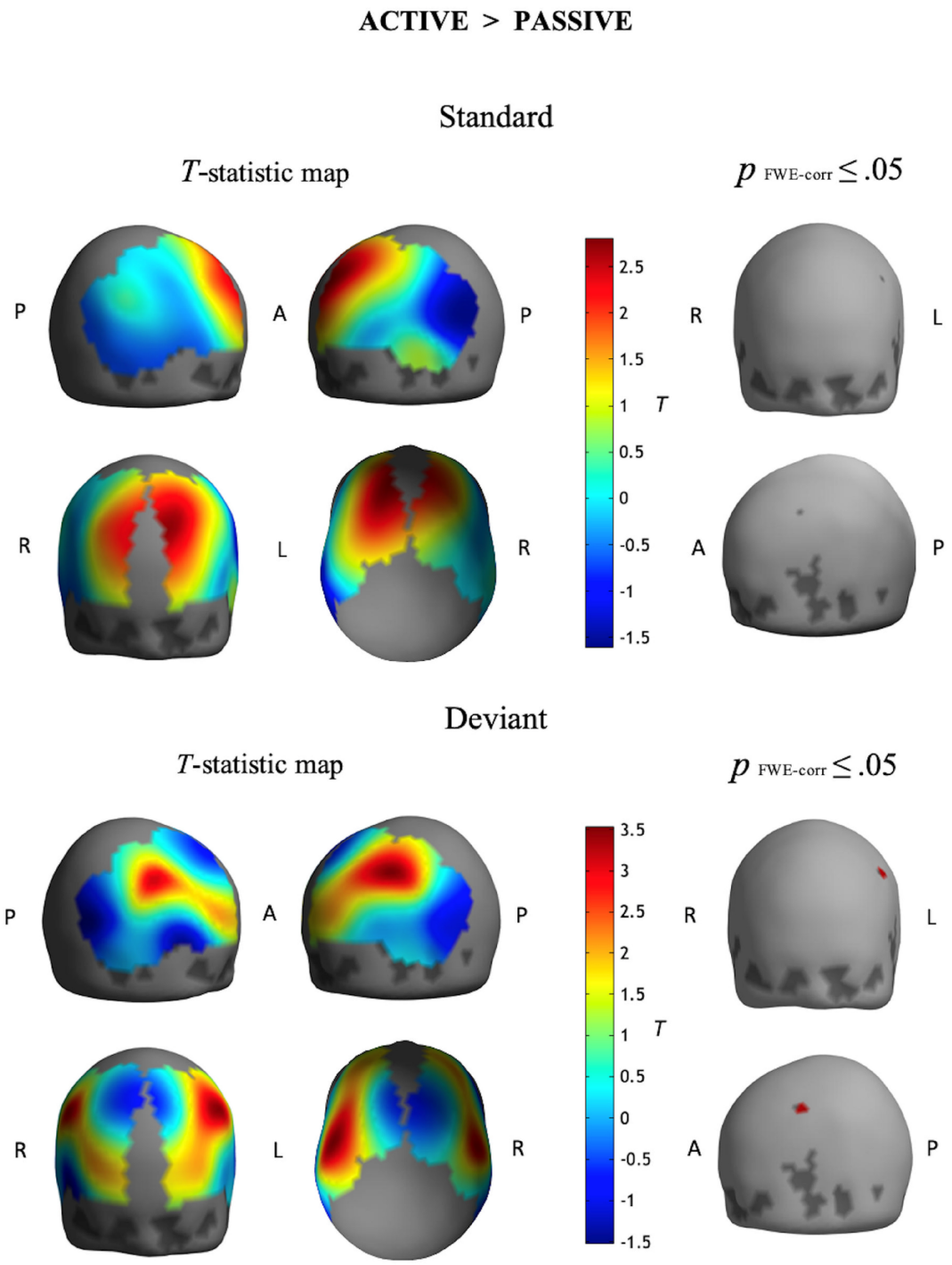

FIGURE 7 T-statistic maps unthresholded (left) and thresholded at *p* FWE-corr <.05 (right), derived from Active > Passive contrast images, respectively, and computed from the HbO responses for standard and deviant trials, respectively. Notice the HbO concentration superiority in regions corresponding to left middle frontal gyrus (MFG) for the active condition. A: anterior; P: posterior; L: left; R: right.

system hierarchically arranged, whereby the MMN and P300 would represent prediction error signals at different processing levels to update the prior brain predictive models.

Contrary to the results reported in other comparative studies between passive and active conditions (Bennington & Polich, 1999; Justen & Herbert, 2018; Näätänen et al., 2011; Wronka et al., 2008), neither the P300 was found in the passive condition nor the MMN in the active condition. The absence of the P300 component has been previously reported in passive oddball paradigms (Horváth et al., 2008; Rinne et al., 2006) and is consistent with recent results from our group using a similar experimental paradigm (Ruiz-Martínez et al., 2021), but the

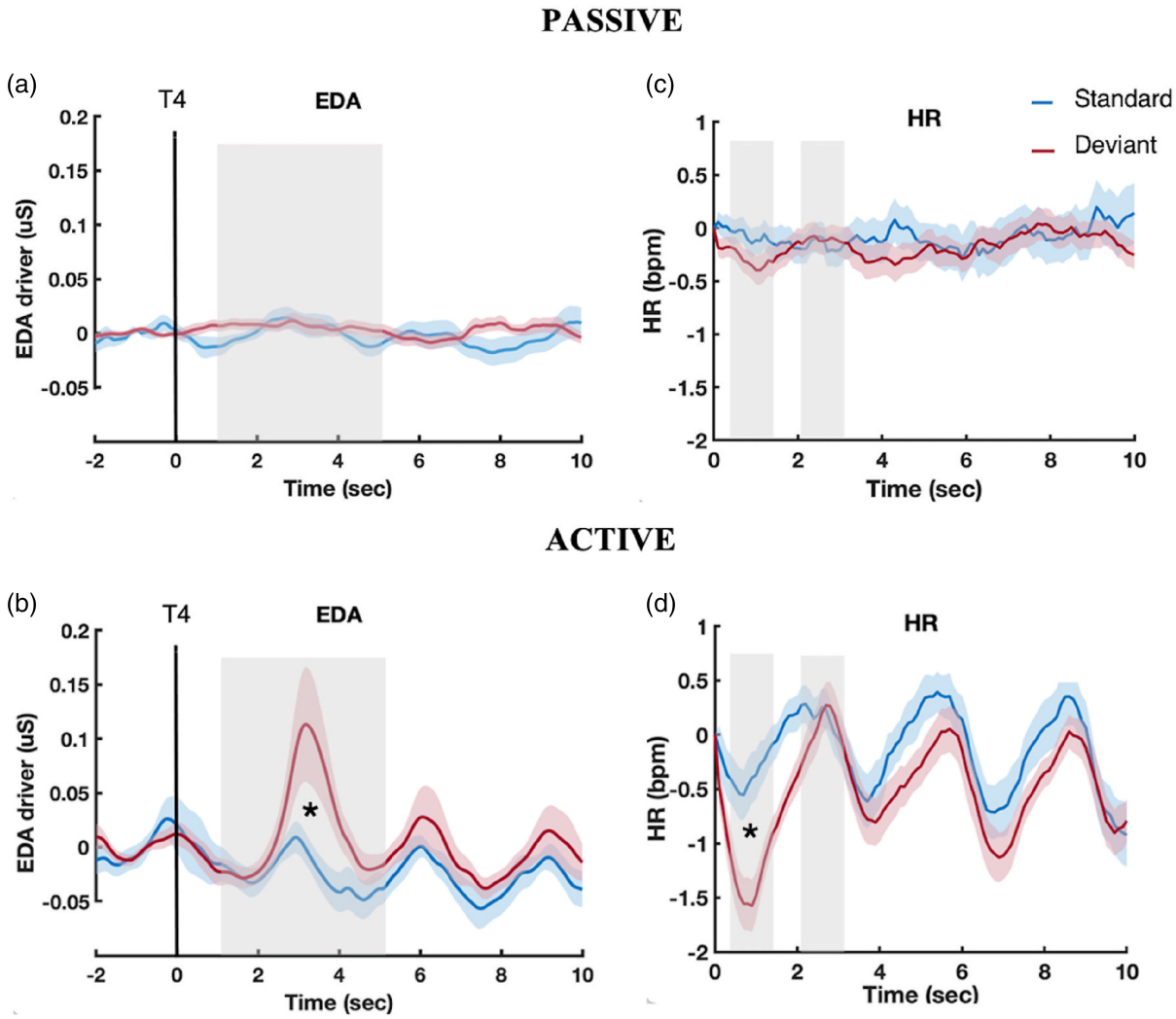

FIGURE 8 (a and b) Electrodermal activity driver signal (EDA) and (C and d) heart rate changes (HR) for the 10 s time window post-T4 stimulus in the passive (top) and active (bottom) conditions, respectively. Shaded gray areas represent the analyzed time window for each signal. Asterisks indicate time windows where significant statistical differences were found. The blue- and red-shaded areas represent the standard error (SE) for standard and deviant trials, respectively.

absence of the MMN in the active condition is an unconventional result that requires further analysis.

Possible hypothetical explanations for the discrepancies with other comparative studies are, on one hand, the different oddball paradigms used (Althen et al., 2013) and, on the other hand, the different instructions given to the participants (Erlbeck et al., 2014). Regarding the different oddball paradigms, a classical oddball paradigm has often been used in other studies, in which the physical features of the deviant stimuli alone could exert a higher salience for an involuntary attentional shift and the P300 elicitation. In contrast, our study utilized a higher complexity oddball paradigm based on auditory patterns, where both congruent and incongruent stimuli shared the same physical properties, thus ruling out discriminability based on the physical properties of the tones. Concerning the instructions given to the participants, some other studies lack any other distractor or competing attentional input in the passive condition, which could compromise the notion of unattended auditory processing and could explain the appearance of the P300 as an attention shift to sound changes, whereas in the passive condition of the present experiment, the participants were instructed to watch a mute film and not to pay attention to the tones. In the active condition, many other oddball studies ask the participants to make a cognitive or motor response only after the arrival of deviant stimuli, and not for the standards, whereas in the present study, the participants were asked to make a motor response by pressing one or another key of the keyboard in each of the trials (standard and deviant), thus equating the motor execution demands of both types of trials within a continuously demanding task, in which a hypothetical greater allocation of attentional resources to task-relevant targets could attenuate or mask

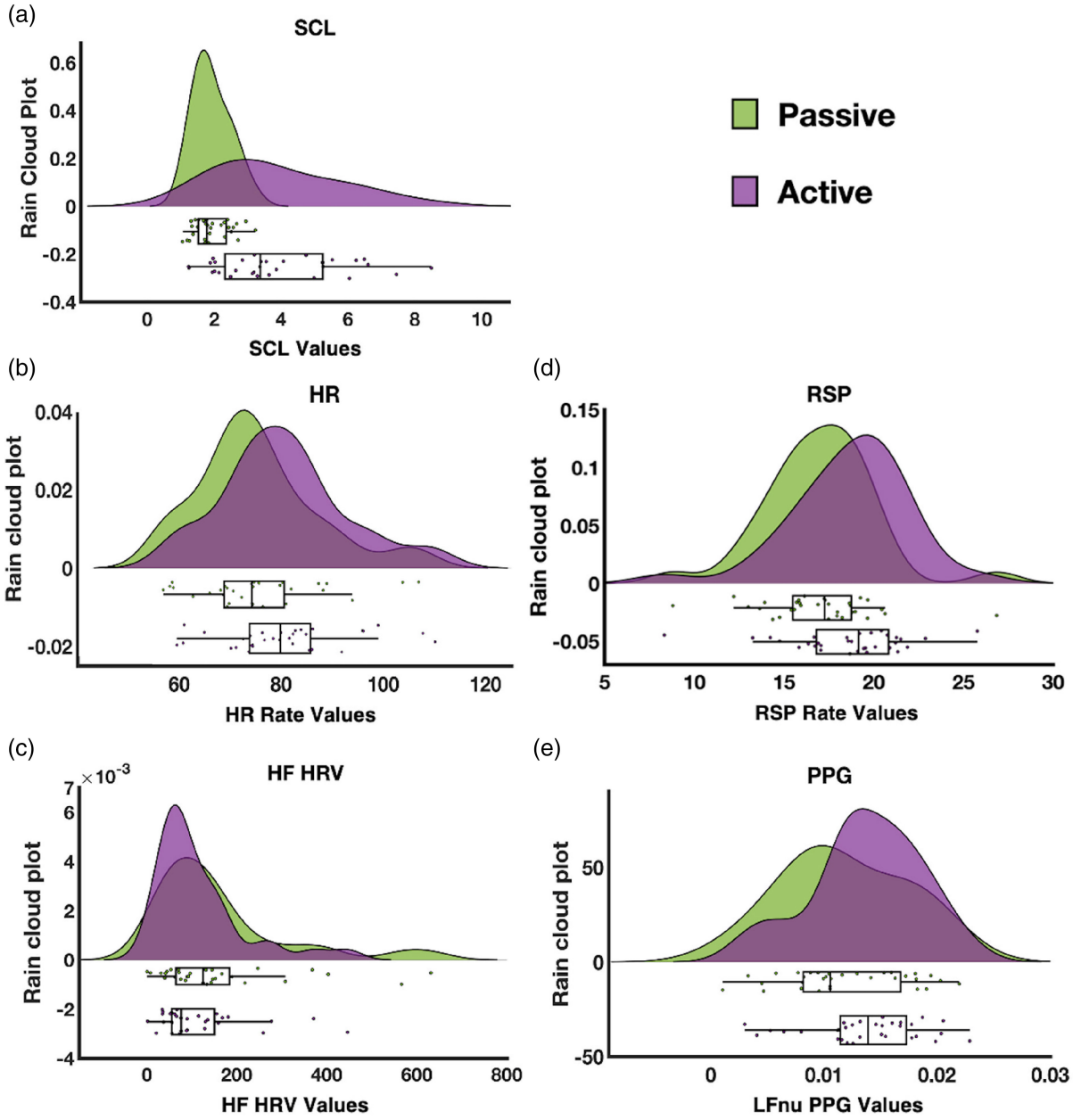

FIGURE 9 Rain cloud plot for the active and passive conditions differences: (a) skin conductance level (SCL) of the electrodermal tonic activity, (b) heart rate (HR), (c) high frequency of the heart rate variability (HRV), (d) respiration rate (RSP), and (e) Low frequency of the peripheral pulse (PPG).

the MMN response as a consequence of a robust P300 component. This possible explanation is congruent with the fNIRS results found and will be further discussed.

Interestingly, in the long latency ERP analysis, CNV and PINV were found in both the active and passive conditions with a similar morphology in the time course domain, although with a higher amplitude in the active condition for the CNV. These results are consistent with previous findings from our group (Ruiz-Martínez et al., 2021, 2022) and, by adding the active condition comparison, provide an additional level of empirical support for the view of these slow evoked potentials as brain predictive coding phenomena, elicited even under unattended auditory stimulation. Moreover, this finding highlights the predictive brain processes of anticipation (CNV) and updating (PINV), respectively, as shared automatic predictive coding phenomena in passive and active conditions. The larger amplitude for the active condition in CNV could be interpreted as a greater allocation of neural resources in the face of task performance demands. The presence of a PINV in both conditions reinforces previous ideas about the role of this component in reappraisal of contingency relationships in uncertain situations (Elbert et al., 1982).

The early negativity in the previously considered PINV could also represent a reorienting negativity ERP component (RON), peaking around 400–450 ms post-deviant stimulus. This negativity was found in both the active and passive conditions, supporting the notion of common reorienting processes, independent of conscious attentional effort to the auditory stimulus. This result is congruent with other studies using complex oddball paradigms that found a similar negative deflection in this time window, also reported as *complex* MMN, *late* MMN, or *late discriminative negativity* (LDN) (Haigh, 2020; Wetzel & Schröger, 2014; Zachau et al., 2005). Additionally, the absence of the P300 and MMN in the passive and active conditions, respectively, together with the shared RON in both conditions, reinforces the conception of the MMN, P300, and RON as dissociated ERPs (Horváth et al., 2008). Another aspect of further research would be whether the RON component could be interpreted as part of the PINV, as reflecting the same response, or as a differentiated ERP.

TABLE 1 Loading components of the nine variables included in the principal component analysis.

	Extracted components			
Variables	**C1**	**C2**	**C3**	**C4**
ERP_CNV_FCz	.117	**.732**	−.057	−.243
ERP_PINV_FCz	.111	**.843**	−.064	.050
fNIRS_HbO_R_STG	−.043	−.082	**.779**	−.216
fNIRS_HbO_L_STG	.203	.057	**.792**	.122
fNIRS_HbO_R_MFG	**.810**	.070	.086	.044
fNIRS_HbO_L_MFG	**.818**	−.002	.176	.093
fNIRS_HbO_FP	**.580**	−.044	−.112	−.391
ANS_HR_PCR	−.362	**.607**	.135	.065
ANS_EDA_SCR	.027	−.102	−.107	**.901**
Explained variance	20.7	18.2	14.7	12.2

Note: In bold are the loading components ≥0.51.

4.3 | Functional near-infrared spectroscopy

In the fNIRS analysis of cortical hemodynamic activity, a distinct and dissociated topographic activation was found for each condition, with an overall higher-amplitude HbO response for the active condition.

In the passive condition, no significant HbO response was found for standard events, whereas a significant increase in HbO concentration was found for deviant events on the right STG, and a trend was found in the left STG. This temporal cortical activation can be associated with the MMN shown in the EEG analysis, which is consistent with previous MMN source localization studies using EEG and/or fMRI that point to the STG and IFG as the main cortical MMN generators (Garrido et al., 2008; Li et al., 2019; Molholm et al., 2005; Opitz et al., 2002).

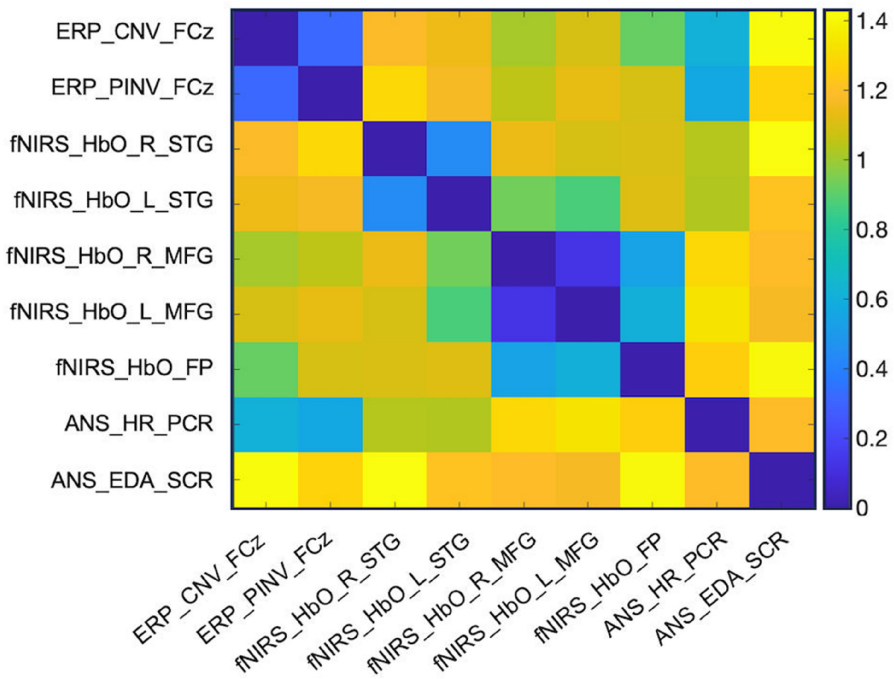

FIGURE 10 Euclidean distances from the loading components of the nine variables included in the principal components analysis. Lower values (blue) indicate lower Euclidean distance between variables in the four-dimensional space generated by the four selected principal components.

However, in contrast to the mentioned evidence on MMN generators, activation of the IFG did not reach significant HbO concentration changes in the present work. To explain the lack of recorded HbO response on the IFG, it is important to note that, to the best of our knowledge, this is the first attempt to address the MMN elicitation with the fNIRS neuroimaging technique, and despite its ecological advantages and tested applications for cognitive neuroscience, some technical limitations inherent to fNIRS for capturing hemodynamic activity in certain cortical regions should not be discarded compared to fMRI studies (Quaresima & Ferrari, 2019; Felix Scholkmann et al., 2014).

In the active condition, a significant increase in HbO concentration was found in the left medial frontopolar cortex for standard events. Activation of this cortical area has been associated, within the predictive coding framework, with the resolution of uncertainty by confirming and maintaining our prior beliefs from available observations in sequential decision tasks (Yoshida & Ishii, 2006), which is congruent with the conception of standards (80% trials) as the expected events under the present experimental paradigm. For deviant events, a significant increase in HbO concentration was found bilaterally on middle frontal gyrus (MFG), but with greater amplitude in the left hemisphere. MFG activation has been previously reported with fMRI in other studies using cueing tasks (Japee et al., 2015; Thiel et al., 2004), and it has been interpreted as the emergence of working memory processes reflecting the evaluation of unexpected stimuli (Corbetta et al., 2002) or the inhibition of premature responses due to the high predictiveness of the cues (Arrington et al., 2000; Vossel et al., 2006). Within the predictive coding framework, the MFG activation could reflect the error representation updating in the working memory to generate better estimates of likely action outcomes for optimal task performance (Alexander & Brown, 2015), which would be in line with the P300 explanation as a higher-order prediction error signal in a top–down hierarchical process.

A right hemisphere predominance was found in the passive condition for MMN elicitation, consistent with the existing evidence on MMN generation (Levänen et al., 1996; Recasens & Uhlhaas, 2017; Wang et al., 2021). However, active condition induced a predominant frontal left activation. This swap in the brain dominant hemisphere between passive and active auditory processing replicated results from Wang et al. (2021) and could indicate a hemispheric redistribution of hierarchical attentional resources, ranging from right-hemisphere specialization in early auditory processing to left-hemisphere superiority in later or higher-order auditory processing.

The MFG activation in response to deviant events for the active condition could be associated with the P300 in the EEG analysis, which is congruent with the frontal and parietal P300 generation reported in consistent previous fMRI studies (Horovitz et al., 2002; Linden et al., 1999; Mccarthy et al., 1997) and other fMRI studies using a visual equivalent task such as the Posner cueing task (Thiel et al., 2004). However, an important limitation of this study was that the fNIRS optodes configuration only covered temporal and frontal cortical areas, which did not allow the observation of the brain hemodynamic responses in other cortical regions, such as parietal cortex, that have been consistently associated with the P300 generation. Likewise, as fNIRS measurements are limited to superficial cortical brain regions, the response of deeper brain regions could not be explored.

Curiously, neither significant cortical hemodynamic activity was found in the STG for the active condition as found in the passive condition, nor significant cortical hemodynamic activity was found in the MFG for the passive condition as found in the active condition. Conversely, a differential topographic activation pattern between frontal and temporal cortex was observed for each condition. This dissociated cortical hemodynamic activity is in consonance with the distinct ERPs found for the passive and active conditions and might indicate a hierarchical optimization and redistribution of the brain neural processing resources to different cortical regions depending on the contextual demands of the task.

4.4 | Peripheral signals

In the ANS response analyses, EDA measured from the SCR showed significantly higher amplitudes for deviant trials in the active condition, whereas in the passive condition, consistent with the classic results of Lyytinen et al. (1992), no ANS response was associated with MMN, supporting the proposition that MMN elicitation is independent of ANS responses and conscious perception. The increase in SCR can be considered as a sympathetic response typical of an orienting response (Kenemans et al., 1989).

Similarly, as proposed by Simons et al. (1998) and Guerra et al. (2016), an early deceleration in the HR was found in response to deviant trials only for the active condition. The early HR deceleration is also a typical component of the orienting response, also described as early cardiac response (ECR1), as a correlate of the stimulus registration (MacDonald & Barry, 2017). The latter aspect is clearly evident in the post-deviant standard trial which also presents a deceleration–acceleration pattern. However, the acceleration peak did not show a standard–deviant effect, which could be due to the fact that the inter-trial time in these studies is longer

than that used in the present study but also the overlapping time of the acceleration response with the next presented trial could have a damping effect on the cardiac acceleration response.

The significant deceleration of HR and increase in SCR for deviant trials in the active condition, in which frontal activation and P300 are elicited, could reflect that conscious perception leading to imperative responses is accompanied by phasic ANS responses to auditory pattern violation in a hierarchical top–down process that prepares the organism to reach optimal levels of arousal to exert an accurate performance on the task.

Given the results obtained on the SCR and HR signals in the standard–deviant comparison, it is difficult to distinguish these results as a substantial part of predictive coding theory, or as the more classical phenomenon of the orienting response (Sokolov, 1990). If the latter perspective is taken, the ANS response to deviants should be considered as an arousal regulation from an attentional shift to a mismatch of the memory trace of previous stimuli, rather than an active predictive inference violation. However, if these body ANS signals can be reafferented to the CNS to facilitate prior updating is something that should need further research. In such case, the functional system theory, in the comparison between the acceptor and the reafferent signal, should be considered (Anokhin, 1974). A sequential Bayesian modeling analysis of ANS responses could be a potential analytical tool to analyze such possibility, as it has been applied to demonstrate the relationship of CNV with priors and P300 with prediction error (Gómez et al., 2019).

On the other hand, continuous autonomic measures of EDA (both SCL and SCR), HR, and RSP rate showed higher amplitudes throughout the active condition, compared to the passive condition, indicating a higher ANS sympathetic activation integrated with greater and distinctive brain responses for the active condition, compared with the passive condition. The PPG LFnu power has recently been proposed as a marker of peripheral vascular tone (Bernardi et al., 1996; Karavaev et al., 2021; Kiselev & Karavaev, 2020; Muñoz et al., 2022). In the present study, consistent with the other ANS measurements, the higher LFnu power for the active condition suggests sympathetic control of vascular tone during the attentional process. In the same line, vagal or parasympathetic control could be indicated by the higher values of HF in the HRV analysis for the passive condition. Overall, these results could suggest a systemic and interdependent process of optimization of the neural resources and arousal levels proportionally to the contextual demands of the task.

Lastly, in EDA and HR response for the active condition, rhythmic waves tuned to 3-second cycles that correspond to the auditory stimulation pattern were found, which could be a manifestation of ANS response synchronization to repetitive sensorial stimulation, or a continuous registration with low habituation of the repetitively presented trials (MacDonald & Barry, 2017). Nevertheless, a more detailed analysis of this finding exceeds the scope of the present research and will remain pending for future research.

4.5 | Principal component analysis

The autonomic variables included in the PCA produced a limited pattern of covariation with the CNS. Only variability of the HR deceleration was associated with the amplitude of the slow ERPs (CNV and PINV). In fact, the early CNV has classically been related to an orienting response (Loveless & Sanford, 1974), as it has also been the HR deceleration (Kenemans et al., 1989).

Given the simultaneity of CNV and PINV with the HR decelerative responses, if any causal relationship should be inferred, a directionality of the frontal components involved in the generation of these slow ERP components over the ANS system would be a more probable hypothesis than a reafference of ANS to CNS (Gómez et al., 2003). On the other hand, the lack of common variance between ANS and fNIRS signals should be due to the analysis pipeline, particularly the use of short channels as regressors and the elimination of the first principal component, which by improving the hemodynamic response certainly would also diminish the autonomic influence of the processed fNIRS signal. However, the unexpected results of a lack of neurovascular coupling between ERPs and fNIRS can parsimoniously be explained by a lack of signal sensitivity, different reactivity for different signals, or a reduced variance between subjects. Finally, the independence in the sources of variability between STG and frontal fNIRS signals suggests an independent coding of higher- versus lower-order processing of the presented auditory sequences.

5 | CONCLUSIONS

The results show shared slow evoked potentials between the passive and active conditions that could be interpreted as predictive processes of anticipation and updating, independent of conscious attentional effort, supporting the view of the brain as a continuously active inferential system sustained by the predictive coding framework. A dissociated topography of the cortical hemodynamic activity and distinctive evoked potentials upon auditory pattern violation were also found between both conditions, whereas only conscious perception

leading to imperative responses was accompanied by phasic ANS responses. These results suggest a systemic-level hierarchical reallocation of predictive coding neural resources as a function of contextual demands in the face of sensory stimulation. This systemic neurophysiological approach could potentially be applied to provide new findings in mental disorders where underlying predictive coding dysfunction has been proposed, such as schizophrenia.

AUTHOR CONTRIBUTIONS

Manuel Muñoz-Caracuel: Conceptualization; data curation; formal analysis; visualization; writing – original draft. **Vanesa Muñoz:** Data curation; formal analysis; writing – original draft. **Francisco J. Ruiz-Martínez:** Data curation; formal analysis; writing – original draft. **Antonio J. Vázquez Morejón:** Investigation; validation. **Carlos Gómez:** Conceptualization; data curation; supervision; writing – review and editing.

ACKNOWLEDGMENTS

The authors thank all the participants in the experiment for their collaboration, time, and patience to help in the present study.

FUNDING INFORMATION

This study was supported by the Spanish Agencia Estatal de Investigación (AEI) (PID2022-139151OB-I00) (FEDER funds) and by the Consejería de Innovación, Ciencia y Empresa of the Junta de Andalucía (P20_00537).

CONFLICT OF INTEREST STATEMENT

The authors declare no competing interests.

DATA AVAILABILITY STATEMENT

The data that support the findings of this study are available from the corresponding author (mmunoz41@us.es) upon reasonable request.

ORCID

Manuel Muñoz-Caracuel https://orcid.org/0000-0003-1667-5646

REFERENCES

Alexander, W. H., & Brown, J. W. (2015). Hierarchical error representation: A computational model of anterior cingulate and dorsolateral prefrontal cortex. *Neural Computation*, *27*(11), 2354–2410. https://doi.org/10.1162/NECO_A_00779

Allen, M., & Friston, K. J. (2018). From cognitivism to autopoiesis: Towards a computational framework for the embodied mind. *Synthese*, *195*(6), 2459–2482. https://doi.org/10.1007/S11229-016-1288-5/FIGURES/4

Althen, H., Grimm, S., & Escera, C. (2013). Simple and complex acoustic regularities are encoded at different levels of the auditory hierarchy. *The European Journal of Neuroscience*, *38*(10), 3448–3455. https://doi.org/10.1111/EJN.12346

Anokhin, P. K. (1974). *Biology and neurophysiology of the conditioned reflex and its role in adaptive behavior*. Elsevier.

Arjona, A., Escudero, M., & Gómez, C. M. (2014). Updating of attentional and premotor allocation resources as function of previous trial outcome. *Scientific Reports*, *4*, 1–9. https://doi.org/10.1038/SREP04526

Arrington, C. M., Carr, T. H., Mayer, A. R., & Rao, S. M. (2000). Neural mechanisms of visual attention: Object-based selection of a region in space. *Journal of Cognitive Neuroscience*, *12*(Supplement 2), 106–117. https://doi.org/10.1162/089892900563975

Benedek, M., & Kaernbach, C. (2010). A continuous measure of phasic electrodermal activity. *Journal of Neuroscience Methods*, *190*(1), 80–91. https://doi.org/10.1016/J.JNEUMETH.2010.04.028

Bennington, J. Y., & Polich, J. (1999). Comparison of P300 from passive and active tasks for auditory and visual stimuli. *International Journal of Psychophysiology*, *34*(2), 171–177. https://doi.org/10.1016/S0167-8760(99)00070-7

Bernardi, L., Radaelli, A., Solda, P. L., Coats, A. J. S., Reeder, M., Calciati, A., Garrard, C. S., & Sleight, P. (1996). Autonomic control of skin microvessels: Assessment by power spectrum of photoplethysmographic waves. *Clinical Science*, *90*(5), 345–355. https://doi.org/10.1042/CS0900345

Boucsein, W., Fowles, D. C., Grimnes, S., Ben-Shakhar, G., Roth, W. T., Dawson, M. E., & Filion, D. L. (2012). Publication recommendations for electrodermal measurements. *Psychophysiology*, *49*(8), 1017–1034. https://doi.org/10.1111/J.1469-8986.2012.01384.X

Brigadoi, S., Ceccherini, L., Cutini, S., Scarpa, F., Scatturin, P., Selb, J., Gagnon, L., Boas, D. A., & Cooper, R. J. (2014). Motion artifacts in functional near-infrared spectroscopy: A comparison of motion correction techniques applied to real cognitive data. *NeuroImage*, *85*, 181–191. https://doi.org/10.1016/J.NEUROIMAGE.2013.04.082

Cooper, R. J., Selb, J., Gagnon, L., Phillip, D., Schytz, H. W., Iversen, H. K., M. Ashina & Boas, D. A. (2012). A systematic comparison of motion artifact correction techniques for functional near-infrared spectroscopy. *Frontiers in Neuroscience*, *6*, 32692. https://doi.org/10.3389/FNINS.2012.00147/BIBTEX

Corbetta, M., Kincade, J. M., & Shulman, G. L. (2002). Neural Systems for Visual Orienting and Their Relationships to spatial working memory. *Journal of Cognitive Neuroscience*, *14*(3), 508–523. https://doi.org/10.1162/089892902317362029

Elbert, T., Rockstroh, B., Lutzenberger, W., & Birbaumer, N. (1982). Slow brain potentials after withdrawal of control. *Archiv für Psychiatrie und Nervenkrankheiten*, *232*(3), 201–214. https://doi.org/10.1007/BF02141781/METRICS

Erlbeck, H., Kübler, A., Kotchoubey, B., & Veser, S. (2014). Task instructions modulate the attentional mode affecting the auditory MMN and the semantic N400. *Frontiers in Human Neuroscience*, *8*, 654. https://doi.org/10.3389/FNHUM.2014.00654

Escera, C., & Corral, M. J. (2007). Role of mismatch negativity and novelty-P3 in involuntary auditory attention. *Journal of Psychophysiology*, *21*(3–4), 251–264. https://doi.org/10.1027/0269-8803.21.34.251

Ficco, L., Mancuso, L., Manuello, J., Teneggi, A., Liloia, D., Duca, S., Costa, T., Kovacs, G. Z., & Cauda, F. (2021). Disentangling

predictive processing in the brain: A meta-analytic study in favour of a predictive network. *Scientific Reports*, *11*(1), 1–14. https://doi.org/10.1038/s41598-021-95603-5

Fitzgerald, K., & Todd, J. (2020). Making sense of mismatch negativity. *Frontiers in Psychiatry*, *11*, 1–19. https://doi.org/10.3389/fpsyt.2020.00468

Friston, K. (2010). The free-energy principle: A unified brain theory? *Nature Reviews Neuroscience*, *11*(2), 127–138. https://doi.org/10.1038/nrn2787

Garrido, M. I., Friston, K. J., Kiebel, S. J., Stephan, K. E., Baldeweg, T., & Kilner, J. M. (2008). The functional anatomy of the MMN: A DCM study of the roving paradigm. *NeuroImage*, *42*(2), 936–944. https://doi.org/10.1016/j.neuroimage.2008.05.018

Garrido, M. I., Kilner, J. M., Stephan, K. E., & Friston, K. J. (2009). The mismatch negativity: A review of underlying mechanisms. *Clinical Neurophysiology*, *120*(3), 453–463. https://doi.org/10.1016/j.clinph.2008.11.029

Gómez, C. M., Marco, J., & Grau, C. (2003). Preparatory visuo-motor cortical network of the contingent negative variation estimated by current density. *NeuroImage*, *20*(1), 216–224. https://doi.org/10.1016/S1053-8119(03)00295-7

Gómez, C. M., Arjona, A., Donnarumma, F., Maisto, D., Rodríguez-Martínez, E. I., & Pezzulo, G. (2019). Tracking the time course of Bayesian inference with event-related potentials: A Study using the central cue Posner paradigm. *Frontiers in Psychology*, *10*, 1424. https://doi.org/10.3389/FPSYG.2019.01424

Gorsuch, R. L. (1983). *Factor analysis* (2nd ed.). W.B. Saunders Company. http://www.amazon.com/Factor-Analysis-Edition-Richard-Gorsuch/dp/089859202X?SubscriptionId=0NM5T5X751JWT17C4GG2&tag=sonnysoftware&linkCode=xm2&camp=2025&creative=165953&creativeASIN=089859202X

Grent-'t-Jong, T., & Uhlhaas, P. J. (2020). The many facets of mismatch negativity. *Biological Psychiatry*, *87*(8), 695–696. https://doi.org/10.1016/j.biopsych.2020.01.022

Guerra, P. M., Sánchez-Adam, A., Miccoli, L., Polich, J., & Vila, J. (2016). Heart rate and P300: Integrating peripheral and central indices of cognitive processing. *International Journal of Psychophysiology*, *100*, 1–11. https://doi.org/10.1016/J.IJPSYCHO.2015.12.008

Haigh, S. M. (2020). Reductions in complex mismatch negativity to extra tone gestalt pattern deviance in first-episode schizophrenia. *Frontiers in Psychiatry*, *11*, 1–9. https://doi.org/10.3389/fpsyt.2020.00505

Hair, J. F., Anderson, R. E., Tatham, R. L., & Black, W. C. (1998). *Multivariate data analysis*. Prentice Hall. https://dialnet.unirioja.es/servlet/libro?codigo=374900

Helmholtz H. von. (1867). Handbuch der physiologischen optik. Voss.

Hohwy, J. (2012). Attention and conscious perception in the hypothesis testing brain. *Frontiers in Psychology*, *3*, 96. https://doi.org/10.3389/FPSYG.2012.00096/BIBTEX

Horovitz, S. G., Skudlarski, P., & Gore, J. C. (2002). Correlations and dissociations between BOLD signal and P300 amplitude in an auditory oddball task: A parametric approach to combining fMRI and ERP. *Magnetic Resonance Imaging*, *20*(4), 319–325. https://doi.org/10.1016/S0730-725X(02)00496-4

Horváth, J., Winkler, I., & Bendixen, A. (2008). Do N1/MMN, P3a, and RON form a strongly coupled chain reflecting the three stages of auditory distraction? *Biological Psychology*, *79*(2), 139–147. https://doi.org/10.1016/j.biopsycho.2008.04.001

Hsu, Y. F., Le Bars, S., Hämäläinen, J. A., & Waszak, F. (2015). Distinctive representation of mispredicted and unpredicted prediction errors in human electroencephalography. *Journal of Neuroscience*, *35*(43), 14653–14660. https://doi.org/10.1523/JNEUROSCI.2204-15.2015

Huppert, T. J., Diamond, S. G., Franceschini, M. A., & Boas, D. A. (2009). HomER: A review of time-series analysis methods for near-infrared spectroscopy of the brain. *Applied Optics*, *48*(10), D280–D298. https://doi.org/10.1364/AO.48.00D280

Ishbulatov, Y. M., Karavaev, A. S., Kiselev, A. R., Simonyan, M. A., Prokhorov, M. D., Ponomarenko, V. I., Mironov, S. A., Gridnev, V. I., Bezruchko, B. P., & Shvartz, V. A. (2020). Mathematical modeling of the cardiovascular autonomic control in healthy subjects during a passive head-up tilt test. *Scientific Reports*, *10*(1), 1–11. https://doi.org/10.1038/s41598-020-71532-7

Jääskeläinen, I. P., Ahveninen, J., Bonmassar, G., Dale, A. M., Ilmoniemi, R. J., Levänen, S., Lin, F. H., May, P., Melcher, J., Stufflebeam, S., Tiitinen, H., & Belliveau, J. W. (2004). Human posterior auditory cortex gates novel sounds to consciousness. *Proceedings of the National Academy of Sciences of the United States of America*, *101*(17), 6809–6814. https://doi.org/10.1073/PNAS.0303760101

Japee, S., Holiday, K., Satyshur, M. D., Mukai, I., & Ungerleider, L. G. (2015). A role of right middle frontal gyrus in reorienting of attention: A case study. *Frontiers in Systems Neuroscience*, *9*, 122128. https://doi.org/10.3389/FNSYS.2015.00023/ABSTRACT

Justen, C., & Herbert, C. (2018). The spatio-temporal dynamics of deviance and target detection in the passive and active auditory oddball paradigm: A sLORETA study. *BMC Neuroscience*, *19*(1), 1–19. https://doi.org/10.1186/s12868-018-0422-3

Karavaev, A. S., Borovik, A. S., Borovkova, E. I., Orlova, E. A., Simonyan, M. A., Ponomarenko, V. I., Skazkina, V. V., Gridnev, V. I., Bezruchko, B. P., Prokhorov, M. D., & Kiselev, A. R. (2021). Low-frequency component of photoplethysmogram reflects the autonomic control of blood pressure. *Biophysical Journal*, *120*(13), 2657–2664. https://doi.org/10.1016/J.BPJ.2021.05.020

Kathmann, N., Jonitz, L., & Engel, R. R. (1990). Cognitive determinants of the Postimperative negative variation. *Psychophysiology*, *27*(3), 256–263. https://doi.org/10.1111/J.1469-8986.1990.TB00380.X

Kenemans, J. L., Verbaten, M. N., Roelofs, J. W., & Slangen, J. L. (1989). "Initial-" and "change-orienting reactions": An analysis based on visual single-trial event-related potentials. *Biological Psychology*, *28*(3), 199–226. https://doi.org/10.1016/0301-0511(89)90001-X

Kim, H. (2014). Involvement of the dorsal and ventral attention networks in oddball stimulus processing: A meta-analysis. *Human Brain Mapping*, *35*(5), 2265–2284. https://doi.org/10.1002/HBM.22326

Kiselev, A. R., & Karavaev, A. S. (2020). The intensity of oscillations of the photoplethysmographic waveform variability at frequencies 0.04-0.4 Hz is effective marker of hypertension and coronary artery disease in males. *Blood Pressure*, *29*(1), 55–62. https://doi.org/10.1080/08037051.2019.1645586

Klein, C., Rockstroh, B., Cohen, R., Berg, P., & Dressel, M. (1996). The impact of performance uncertainty on the postimperative negative variation. *Psychophysiology*, *33*(4), 426–433. https://doi.org/10.1111/J.1469-8986.1996.TB01068.X

Knill, D. C., & Pouget, A. (2004). The Bayesian brain: The role of uncertainty in neural coding and computation. *Trends in*

Neurosciences, *27*(12), 712–719. https://doi.org/10.1016/j.tins.2004.10.007

Korzyukov, O. A., Winkler, I., Gumenyuk, V. I., & Alho, K. (2003). Processing abstract auditory features in the human auditory cortex. *NeuroImage*, *20*(4), 2245–2258. https://doi.org/10.1016/J.NEUROIMAGE.2003.08.014

Levänen, S., Ahonen, A., Hari, R., McEvoy, L., & Sams, M. (1996). Deviant auditory stimuli activate human left and right auditory cortex differently. *Cerebral Cortex*, *6*(2), 288–296. https://doi.org/10.1093/CERCOR/6.2.288

Li, Q., Liu, G., Yuan, G., Wang, G., Wu, Z., & Zhao, X. (2019). Single-trial EEG-fMRI reveals the generation process of the mismatch negativity. *Frontiers in Human Neuroscience*, *13*, 168. https://doi.org/10.3389/fnhum.2019.00168

Linden, D. E. J., Prvulovic, D., Formisano, E., Völlinger, M., Zanella, F. E., Goebel, R., & Dierks, T. (1999). The functional neuroanatomy of target detection: An fMRI study of visual and auditory oddball tasks. *Cerebral Cortex*, *9*(8), 815–823. https://doi.org/10.1093/CERCOR/9.8.815

Loveless, N. E., & Sanford, A. J. (1974). Effects of age on the contingent negative variation and preparatory set in a reaction time task. *Journal of Gerontology*, *29*(1), 52–63. https://doi.org/10.1093/GERONJ/29.1.52

Lyytinen, H., Blomberf, A.-P., & Näätänen, R. (1992). Event related potentials and autonomic responses to a change in unattended auditory stimuli.Pdf. *Psychophysiology*, *29*, 523–534.

MacDonald, B., & Barry, R. J. (2017). Significance and novelty effects in single-trial ERP components and autonomic responses. *International Journal of Psychophysiology*, *117*, 48–64. https://doi.org/10.1016/J.IJPSYCHO.2017.03.007

May, P., Tiitinen, H., Ilmoniemi, R. J., Nyman, G., Taylor, J. G., & Näätänen, R. (1999). Frequency change detection in human auditory cortex. *Journal of Computational Neuroscience*, *6*(2), 99–120. https://doi.org/10.1023/A:1008896417606/METRICS

Mccarthy, G., Luby, M., Gore, J., & Goldman-Rakic, P. (1997). Infrequent events transiently activate human prefrontal and parietal cortex as measured by functional MRI. *Journal of Neurophysiology*, *77*(3), 1630–1634. https://doi.org/10.1152/JN.1997.77.3.1630

Molavi, B., & Dumont, G. A. (2010). Wavelet based motion artifact removal for functional near infrared spectroscopy. 2010 Annual International Conference of the IEEE Engineering in Medicine and Biology Society, EMBC'10, 5–8, Buenos Aires, Argentina https://doi.org/10.1109/IEMBS.2010.5626589

Molholm, S., Martinez, A., Ritter, W., Javitt, D. C., & Foxe, J. J. (2005). The neural circuitry of pre-attentive auditory change-detection: An fMRI study of pitch and duration mismatch negativity generators. *Cerebral Cortex*, *15*(5), 545–551. https://doi.org/10.1093/CERCOR/BHH155

Muñoz, V., Diaz-Sanchez, J. A., Muñoz-Caracuel, M., & Gómez, C. M. (2022). Head hemodynamics and systemic responses during auditory stimulation. *Physiological Reports*, *10*(13), e15372. https://doi.org/10.14814/PHY2.15372

Muñoz-Caracuel, M., Muñoz, V., Ruíz-Martínez, F. J., Di Domenico, D., Brigadoi, S., & Gómez, C. M. (2021). Multivariate analysis of the systemic response to auditory stimulation: An integrative approach. *Experimental Physiology*, *106*(4), 1072–1098. https://doi.org/10.1113/EP089125

Näätänen, R., Gaillard, A. W. K., & Mäntysalo, S. (1978). Early selective-attention effect on evoked potential reinterpreted. *Acta Psychologica*, *42*(4), 313–329. https://doi.org/10.1016/0001-6918(78)90006-9

Näätänen, R., Paavilainen, P., Rinne, T., & Alho, K. (2007). The mismatch negativity (MMN) in basic research of central auditory processing: A review. *Clinical Neurophysiology*, *118*(12), 2544–2590. https://doi.org/10.1016/j.clinph.2007.04.026

Näätänen, R., Kujala, T., & Winkler, I. (2011). Auditory processing that leads to conscious perception: A unique window to central auditory processing opened by the mismatch negativity and related responses. *Psychophysiology*, *48*(1), 4–22. https://doi.org/10.1111/j.1469-8986.2010.01114.x

Näätänen, R., & Winkler, I. (1999). The concept of auditory stimulus representation in cognitive neuroscience. *Psychological Bulletin*, *125*(6), 826–859. https://doi.org/10.1037/0033-2909.125.6.826

Oostenveld, R., Fries, P., Maris, E., & Schoffelen, J. M. (2011). FieldTrip: Open source software for advanced analysis of MEG, EEG, and invasive electrophysiological data. *Computational Intelligence and Neuroscience*, *2011*, 1–9. https://doi.org/10.1155/2011/156869

Opitz, B., Rinne, T., Mecklinger, A., Von Cramon, D. Y., & Schröger, E. (2002). Differential contribution of frontal and temporal cortices to auditory change detection: fMRI and ERP results. *NeuroImage*, *15*(1), 167–174. https://doi.org/10.1006/NIMG.2001.0970

Pan, J., & Tompkins, W. J. (1985). A real-time QRS detection algorithm. *IEEE Transactions on Bio-Medical Engineering*, *32*(3), 230–236. https://doi.org/10.1109/TBME.1985.325532

Peirce, J. W. (2009). Generating stimuli for neuroscience using PsychoPy. *Frontiers in Neuroinformatics*, *2*, 1–8. https://doi.org/10.3389/neuro.11.010.2008

Perakakis, P. (2019). HEPLAB: a Matlab graphical interface for the preprocessing of the heartbeat-evoked potential. https://doi.org/10.5281/ZENODO.2649943

Perakakis, P., Joffily, M., Taylor, M., Guerra, P., & Vila, J. (2010). KARDIA: A Matlab software for the analysis of cardiac interbeat intervals. *Computer Methods and Programs in Biomedicine*, *98*(1), 83–89. https://doi.org/10.1016/J.CMPB.2009.10.002

Posner, M. I. (1980). Orienting of attention. *The Quarterly Journal of Experimental Psychology*, *32*(1), 3–25. https://doi.org/10.1080/00335558008248231

Purdon, P. L., & Weisskoff, R. M. (1998). Effect of temporal autocorrelation due to physiological noise and stimulus paradigm on voxel-level false-positive rates in fMRI. *Human Brain Mapping*, *6*(4), 239–249. https://doi.org/10.1002/(sici)1097-0193(1998)6:4<239::aid-hbm4>3.0.co;2-4

Quaresima, V., & Ferrari, M. (2019). Functional near-infrared spectroscopy (fNIRS) for assessing cerebral cortex function during human behavior in natural/social situations: A concise review. *Organizational Research Methods*, *22*(1), 46–68. https://doi.org/10.1177/1094428116658959

Rao, R. P. N., & Ballard, D. H. (1999). Predictive coding in the visual cortex: A functional interpretation of some extra-classical receptive-field effects. *Nature Neuroscience*, *2*(1), 79–87. https://doi.org/10.1038/4580

Recasens, M., & Uhlhaas, P. J. (2017). Test–retest reliability of the magnetic mismatch negativity response to sound duration and omission deviants. *NeuroImage*, *157*, 184–195. https://doi.org/10.1016/J.NEUROIMAGE.2017.05.064

Rinne, T., Särkkä, A., Degerman, A., Schröger, E., & Alho, K. (2006). Two separate mechanisms underlie auditory change detection and involuntary control of attention. *Brain Research*, *1077*(1), 135–143. https://doi.org/10.1016/J.BRAINRES.2006.01.043

Ruiz-Martínez, F. J., Arjona, A., & Gómez, C. M. (2021). Mismatch negativity and stimulus-preceding negativity in paradigms of increasing auditory complexity: A possible role in predictive coding. *Entropy*, *23*(3), 346. https://doi.org/10.3390/e23030346

Ruiz-Martínez, F. J., Morales-Ortiz, M., & Gómez, C. M. (2022). Late N1 and postimperative negative variation analysis depending on the previous trial history in paradigms of increasing auditory complexity. *Journal of Neurophysiology*, *127*(5), 1240–1252. https://doi.org/10.1152/JN.00313.2021

Saarinen, J., Paavilainen, P., Tervaniemi, M., & Naatanen, R. (1992). Representation of abstract attributes of auditory stimuli in the human brain. *Neuroreport*, *3*, 1149–1151. https://doi.org/10.1097/00001756-199212000-00030

Scholkmann, F., Spichtig, S., Muehlemann, T., & Wolf, M. (2010). How to detect and reduce movement artifacts in near-infrared imaging using moving standard deviation and spline interpolation. *Physiological Measurement*, *31*(5), 649–662. https://doi.org/10.1088/0967-3334/31/5/004

Scholkmann, F., Kleiser, S., Metz, A. J., Zimmermann, R., Mata Pavia, J., Wolf, U., & Wolf, M. (2014). A review on continuous wave functional near-infrared spectroscopy and imaging instrumentation and methodology. *NeuroImage*, *85*(Pt 1), 6–27. https://doi.org/10.1016/J.NEUROIMAGE.2013.05.004

Seth, A. K., & Friston, K. J. (2016). Active interoceptive inference and the emotional brain. *Philosophical Transactions of the Royal Society, B: Biological Sciences*, *371*(1708), 20160007. https://doi.org/10.1098/RSTB.2016.0007

Simons, R. F., Graham, F. K., Miles, M. A., & Balaban, M. T. (1998). Input and central processing expressed in ERP and heart rate changes to rare target and rare nontarget stimuli. *Psychophysiology*, *35*(5), 563–575. https://doi.org/10.1017/S0048577298971566

Sokolov, E. N. (1990). The orienting response, and future directions of its development. *The Pavlovian Journal of Biological Science*, *25*(3), 142–150. https://doi.org/10.1007/BF02974268

Sussman, E. S., Chen, S., Sussman-Fort, J., & Dinces, E. (2014). The five myths of MMN: Redefining how to use MMN in basic and clinical research. *Brain Topography*, *27*(4), 553–564. https://doi.org/10.1007/S10548-013-0326-6

Tak, S., Uga, M., Flandin, G., Dan, I., & Penny, W. D. (2016). Sensor space group analysis for fNIRS data. *Journal of Neuroscience Methods*, *264*, 103–112. https://doi.org/10.1016/J.JNEUMETH.2016.03.003

Tervaniemi, M. (2022). Mismatch negativity–stimulation paradigms in past and in future. *Frontiers in Neuroscience*, *16*, 1025763. https://doi.org/10.3389/FNINS.2022.1025763/BIBTEX

Tervaniemi, M., Maury, S., & Näätänen, R. (1994). Neural representations of abstract stimulus features in the human brain as reflected by the mismatch negativity. *Neuroreport*, *5*, 844–846. https://doi.org/10.1097/00001756-199403000-00027

Thiel, C. M., Zilles, K., & Fink, G. R. (2004). Cerebral correlates of alerting, orienting and reorienting of visuospatial attention: An event-related fMRI study. *NeuroImage*, *21*(1), 318–328. https://doi.org/10.1016/J.NEUROIMAGE.2003.08.044

Vossel, S., Thiel, C. M., & Fink, G. R. (2006). Cue validity modulates the neural correlates of covert endogenous orienting of attention in parietal and frontal cortex. *NeuroImage*, *32*(3), 1257–1264. https://doi.org/10.1016/J.NEUROIMAGE.2006.05.019

Wacongne, C., Labyt, E., Van Wassenhove, V., Bekinschtein, T., Naccache, L., & Dehaene, S. (2011). Evidence for a hierarchy of predictions and prediction errors in human cortex. *Proceedings of the National Academy of Sciences of the United States of America*, *108*(51), 20754–20759. https://doi.org/10.1073/PNAS.1117807108/ASSET/DAC9C788-CFB9-4565-B3B3-65AC6F69F37F/ASSETS/GRAPHIC/PNAS.1117807108FIG03.JPEG

Walter, W. G., Cooper, R., Aldridge, V. J., McCallum, W. C., & Winter, A. L. (1964). Contingent negative variation: An electric sign of sensorimotor association and expectancy in the human brain. *Nature*, *203*(4943), 380–384. https://doi.org/10.1038/203380A0

Wang, X. D., Xu, H., Yuan, Z., Luo, H., Wang, M., Li, H. W., & Chen, L. (2021). Brain hemispheres swap dominance for processing semantically meaningful pitch. *Frontiers in Human Neuroscience*, *15*, 621677. https://doi.org/10.3389/FNHUM.2021.621677

Wetzel, N., & Schröger, E. (2014). On the development of auditory distraction: A review. *PsyCh Journal*, *3*(1), 72–91. https://doi.org/10.1002/PCHJ.49

Winkler, I. (2008). Interpreting the mismatch negativity. *Journal of psychophysiology*, *21*(3–4), 147–163. https://doi.org/10.1027/0269-8803.21.34.147

Wronka, E., Kaiser, J., & Coenen, A. (2008). The auditory P3 from passive and active three-stimulus oddball paradigm. *Acta Neurobiologiae Experimentalis*, *68*, 362–372.

Ye, J. C., Tak, S., Jang, K. E., Jung, J., & Jang, J. (2009). NIRS-SPM: Statistical parametric mapping for near-infrared spectroscopy. *NeuroImage*, *44*(2), 428–447. https://doi.org/10.1016/J.NEUROIMAGE.2008.08.036

Yoshida, W., & Ishii, S. (2006). Resolution of uncertainty in prefrontal cortex. *Neuron*, *50*(5), 781–789. https://doi.org/10.1016/j.neuron.2006.05.006

Zachau, S., Rinker, T., Körner, B., Kohls, G., Maas, V., Hennighausen, K., & Schecker, M. (2005). Extracting rules: Early and late mismatch negativity to tone patterns. *Neuroreport*, *16*(18), 2015–2019. https://doi.org/10.1097/00001756-200512190-00009

SUPPORTING INFORMATION

Additional supporting information can be found online in the Supporting Information section at the end of this article.

Figure S1. Phasic cardiac response (PCR) averaged among conditions, stimuli, and subjects. Note the first negative peak at 0.9 s and the first positive peak at 2.6 s post-stimulus. 0.5 s time window around the peaks was selected for statistical analysis.

Figure S2. Comparison computed for the long time window between the standard and deviant trials for the passive condition. Shaded gray areas represent latencies in which the cluster-mass permutation analysis found significant differences ($p \leq .05$).

Figure S3. Comparison computed for the short time window between the standard and deviant trials for the passive condition. Shaded gray areas represent latencies

in which the cluster-mass permutation analysis found significant differences ($p \leq .05$).

Figure S4. Comparison computed for the long time window between the standard and deviant trials for the active condition. Shaded gray areas represent latencies in which the cluster-mass permutation analysis found significant differences ($p \leq .05$).

Figure S5. Comparison computed for the short time window between the standard and deviant trials for the active condition. Shaded gray areas represent latencies in which the cluster-mass permutation analysis found significant differences ($p \leq .05$).

Figure S6. Comparison computed between the average of the passive and active conditions for the time window from S1 to S4. Shaded gray areas represent latencies in which the cluster-mass permutation analysis found significant differences ($p \leq .05$).

Figure S7. T-statistic maps unthresholded (left) and thresholded at $p < .05$ family-wise error corrected for multiple comparisons (right) derived from Deviant > Standard contrast images computed from the HbO responses for the passive and active condition, respectively.

Figure S8. T-statistic maps unthresholded (left) and thresholded at $p < .05$ family-wise error corrected for multiple comparisons (right) derived from Active > Passive contrast images computed from the HbO responses for standards+deviants and deviants-standards, respectively.

Figure S9. (a) Power spectral density of the pulse signal for the 10 s time window post-stimulus. (b) Power spectral density of the pulse signal for the 720 s time window post-condition. (c) Heart rate for the 720 s time window post-condition. (d) Power spectral density of the heart rate variability for the 720 s time window post-condition. The gray shaded area corresponds to the frequencies selected for the LF ad HF power in the spectral analysis.

How to cite this article: Muñoz-Caracuel, M., Muñoz, V., Ruiz-Martínez, F. J., Vázquez Morejón, A. J., & Gómez, C. M. (2024). Systemic neurophysiological signals of auditory predictive coding. *Psychophysiology*, *00*, e14544. https://doi.org/10.1111/psyp.14544